EXPERIMENTAL STRESS ANALYSIS OF AN I-BEAM WITH A RECTANGULAR WEB CUT-OUT

by

JASBIR SINGH ARORA

B. Sc. in Engineering (Civil) Hons., Panjab University, INDIA, 1964.

A MASTER'S THESIS

submitted in partial fulfillment of the

requirements for the degree

MASTER OF SCIENCE

Department of Civil Engineering

KANSAS STATE UNIVERSITY
Manhattan, Kansas

1967

Approved by:

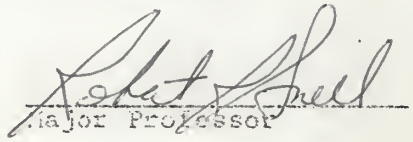

Major Professor

TABLE OF CONTENTS

LIST OF TABLES

LIST OF FIGURES

SUMMARY

In this study, a photostress method of stress analysis was used to investigate the elastic distribution of stresses in an aluminum alloy I-beam with a rectangular web opening at the center. Photostress sheet plastic of type S was used as a birefringent coating. Electric-resistance strain gages were also used at selected places on the flanges and the web. A hydraulic testing machine was used to apply the load at the center of the beam. The load was applied through a 1"x1"x2" rectangular block and a compression load cell was used to record the load.

The photostress readings and strain gage readings were taken at four increments of load. A Large Field Meter was used to take the birefringence and the isoclinic angle readings at different points on a previously selected grid pattern on the plastic. Since most of the readings were between zero and the first fringe, use of the linear compensator and the full wave plate was necessary. All of the strain gages were connected to a Strain Indicator and the readings were recorded with an Automatic Printer. The temperature of the laboratory was maintained at $(68 \pm 2)^{\circ}$ F and the relative humidity was kept relatively constant while making all the observations.

The shear-difference method was used to compute the normal stresses at the interior points of the web. The stresses for a horizontal section were first computed by starting from the free boundary of the hole. The stresses for the various vertical sections were then computed by starting from the corresponding points on that horizontal section. Thus the

elastic stress distribution for five sections of the beam was obtained. The longitudinal stress distribution for section 8 was also obtained from the strain gage readings and that stress distribution was in good agreement with the one obtained from the photostress observations.

Since the conditions assumed in the derivation of the simple theory of flexure were not satisfied in this case the experimental distribution of shear and normal stresses could not be expected to agree with the corresponding distribution of stresses based on simple flexure theory. The neutral axis for the various sections of the beam did not coincide with the centroidal axis of the beam. At section 5 the neutral axis was above the centroidal axis and at section 6 it coincided with the centroidal axis of the beam. At sections 7, 8 and 9 the neutral axis was below the centroidal axis. The curves of shear stress distribution also indicated that the point of maximum shear stress was above the center of the beam at section 5, and at sections 6, 7, 8, 9 and 10 it was below the center line of the beam. By the comparison of the results obtained from the photostress readings and the strain gage readings it was concluded that the shear-difference method of computing stresses at interior points of a member and hence the photostress technique of stress analysis are quite useful in the analysis of such members.

INTRODUCTION

In many practical situations rectangular openings through the webs of structural members such as girders, truss members, ship bulkheads, etc., are required for utility installations or for other purposes. These openings in the webs cause concentration of stresses and the designer is faced with the problem of designing such structural components economically. In all cases, the design must take into consideration the disturbances in the normal stress distribution produced by the presence of discontinuities.

The present study was aimed at studying the effect of a discontinuity in the web on an I-beam subjected to a single concentrated load at the center. Worley (1), Segner (2), and others, have studied this problem. In their studies they investigated wide-flange sections with a series of cut-outs in the webs. However, the present study is concerned with a single rectangular hole in the center of the beam web.

A photo-elastic method of experimental stress analysis, in conjunction with electric-resistance strain gages, was used in the present study. The photo-elastic method provides a very good tool for exploring stresses and strains in many structural components and odd shaped machine parts. Many times these members such as bolt heads, split rings, keys and keyways, toothed gears, grooved beams, etc., cannot be accurately analyzed by other available methods. Photo-stress plastic can be cemented to these members and the directions

of principal strains and the principal strain differences can actually be observed in the laboratory. Thus the distribution of normal stresses across various sections can be obtained in a relatively short time.

The objectives of the present study can be summarized as follows:

(a) To verify the effectiveness of birefringent coatings and the photo-elastic method of stress analysis.

(b) To verify the validity of the shear-difference method in computing the normal stresses at interior points of a structural component.

(c) To study the effect, on stresses, of a hole in the web on an I-beam and to obtain elastic stress distributions at various sections in the beam.

For experimental purposes, an aluminum alloy 6061-T6 I-beam 5"x3" @ 3.43 was selected. A 2"x4" rectangular hole was machined in the web at the center of the beam with the corners of the hole rounded by ½ inch fillets. Then the Photo-stress plastic was carefully machined and cemented around one-half of the hole and extending 7" to one side of it. Strain gages were mounted on the beam flanges to detect and thus avoid eccentric loading. The load was applied through a 1"x1"x2" rectangular steel block. The block was placed longitudinally on the center line of the flange as shown in Fig. 4. A compression load cell was used to measure the load. The strain gages were connected to a Budd Switch and Balance Unit, Digital Strain Indicator, and an Automatic Printer. The Photo-stress

readings were taken with a Large Field Meter and the shear-difference method was used to compute the normal stresses at various sections. The photo-elastic calculations for one particular section were checked by mounting another set of electrical strain gages, on the opposite side of the web, at that section.

REVIEW OF LITERATURE

The photo-elastic method of stress analysis was originated near the beginning of this century. Until approximately 1930 this method did not attain much recognition. In 1935 the Eastern Semi-Annual Conferences on Photo-Elasticity were inaugurated, leading later to the formation of The Society for Experimental Stress Analysis. Since that time a great deal of research has been done in this field.

In 1934, Wahl and Beenwkes studied the concentration of stresses produced by notches (3). The purpose of the study was to find the effect of notches on the member and to study the variation of the stresses in the member.

In a paper published in 1941, Frocht introduced the shear-difference method (18). This method can be used in computing the normal stresses across an arbitrary straight section or along an arbitrary path. It is strictly a photo-elastic method making use of isochromatics, isoclinics, and the differential equations of equilibrium in Cartesian co-ordinates.

In 1949, Hendry investigated the stress distribution in simply supported I-beams.[5] His objective was to study the distribution of stresses and strains under a concentrated central load when it was applied in different ways, i.e., ½" diameter ball, 1" diameter roller wider than flange, 3/4"x 3/4" bar placed lengthways on flange under 1" diameter roller, 1.5"x1" bar placed lengthways, etc. He concluded that:

(a) Stroke's formulas give an adequate representation of stress distributions across the section at the load point for a beam carrying a central concentrated load, (b) that a moderate spread of the load over the flange of the beam is sufficient to reduce the high stresses given by Stroke's formulas and (c) that conventional formulas for calculating the maximum shear stress in the web of a beam apply only at sections farther than about one and a half times the depth of the beam from a point load.

In their publication in 1961, Hendry and Shawki presented a study of the stresses in a deep beam with a centrally concentrated load (6). In that study they confirmed the usefulness of the finite-difference method of analysis of deep beams put forward by Durant and Garwood (6) and by Chow, Conway and Winter (6). They also proved that the theoretical solutions are difficult or impractical where the loading is unsymmetrical or when there are holes in the beams. In those cases the easiest solution was by the photo-elastic method. They also put forward the idea that Wilson-Stroke's theory was misleading and was not applicable for calculation of normal stresses where the span was less than 2.5 times the depth.

In the same year, Worley presented a photo-elastic analysis of wide-flange sections with various types of elliptical web cut-outs (1). The principal objective of the investigation was to establish the elastic stress distribution at the surface of the web cut-outs for various cut-out shapes

when loaded with a central load in bending. He used the shear-difference method to locate the approximate positions of plastic hinges. He also showed that this method gave promising results and could be used effectively. He concluded that the upper or lower flanges and the remaining web material above or below the holes tend to behave as independent T-shaped beams.

Duffy, in the same year, reported on the effects of thickness of birefringent coatings (7). After his investigations he concluded that in the measurement of birefringence two factors should be considered. These were: the strain gradient at the specimen surface and the curvature of the specimen surface under the load. He pointed out that large errors could be expected in certain circumstances where these factors were neglected. He presented the values of the necessary correction factors for different Poisson's ratios.

Again in the year 1961, Post and Zandman studied the accuracy of the birefringent coating method for coatings of arbitrary thickness (8). Some of their conclusions were: (a) for the case of plane-stress problems and equal Poisson's ratio of structure and coating, the influence of coating thickness on birefringence developed along free boundaries was almost zero, (b) for unequal Poisson's ratios, and singly connected structures in plane stress, birefringence developed along free boundary was almost independent of coating thickness, (c) in order to minimize the effects of different Poisson's ratios and local reinforcement they preferred thin

coatings and suggested that, for most engineering problems, 1/8 inch thick coatings would generally be desirable, (d) that plane stress distribution for singly and multiply connected bodies and general surface strain problems could be analyzed effectively by the method of birefringent coating measurement.

Another study on the reinforcing effect of birefringent coatings was made by Redner, Zandman and Reigner in 1962 (9). They developed curves for correction factors applicable to some metal in particular cases such as flexure of plates, torsion of shafts and cylindrical pressure vessels, and combined axial and flexural loads in plates and beams. They also pointed out that the only critical case for the application of a reinforcement correction factor was that of flexure of plates when the plastic was cemented to the surface of the plate. They concluded that in the case of thin coatings no difficulty existed and that the correction factors would be negligibly small. They verified their results by the use of electric-resistance strain gages.

In 1962, Shimada presented results of an investigation of stresses in bars with reinforced semi-circular notches under bending (10). He made this study to determine the type of reinforcement that would change the stress distribution outside the notch to equal the conditions existing in a bar having no notch. A relationship between maximum shear stress and width of bar was obtained and the most suitable types of reinforcements were discussed.

In 1963, Segner made a study of the requirements for reinforcement around large rectangular openings in the webs of wide-flange beams (2). He investigated various beams for different combinations of shear and moment; i.e., low shear and high moment, high shear and moderate moment, high shear and low moment. After examining the test results he concluded that the Vierendeel Truss analogy is an appropriate method of analysis for such problems. He concluded that for any beam containing openings, large deflections should be expected and that where possible the designer should select a deeper section of similar modulus of section. This would sometimes avoid the necessity for reinforcement.

In 1965, Snell reported the results of a study of the reinforcement requirements for plates in uni-axial tension (11). He made use of a birefringent coating technique to verify his theoretical results.

In 1965, Vodivic investigated errors in the analysis of photo-elastic raw data (12). He analyzed errors in the shear-difference method and pointed out that if the data obtained from photo-elastic experiment were accurate, the results computed by this method would also be quite accurate.

BRIEF REVIEW OF THE TWO DIMENSIONAL THEORY OF PHOTO-ELASTICITY

Wave Theory:

According to the electro-magnetic wave theory, light is considered to be a wave whose transverse vibrations take place in any direction in a plane perpendicular to the direction of propagation. An ordinary beam of light contains an infinite number of such waves, each of which has its own transverse vibration.

The wave length and velocity with which the light propagates depend upon the medium through which the light passes. For certain materials the velocity may further depend upon the plane in which light vibrates; i.e., it may propagate with different velocities in different planes. Each monochromatic light wave is specified by the frequency with which it vibrates and it is distinguished from others through the sense of color. The color is a function of frequency rather than of wave length, but it is customary to describe color in terms of the wave length in air. This is feasible because the frequency, n, and the wave length, λ, are related to each other by the following equation:

$$c = \lambda/n \ , \qquad (1)$$

where c is the velocity of light in vacuum.

Light can also be represented by a vector. The magnitude of the vector is equal to the amplitude of vibration and the direction of the vector is that of the vibration.

Thus monochromatic light is represented by a single light vector whereas white light is a combination of several vectors.

One of the most important optical properties employed in the photo-elastic method is the polarization of light. The term polarization may be applied in the sense that some kind of control exists over the light vector or that the vector obeys some definite laws.

Plane Polarization:

Polarized light in which the particles are constrained to vibrate only in parallel planes is said to be plane polarized; i.e., the vibration is allowed only in one direction. In this case the light vector has a constant direction, though its magnitude may change.

Circular Polarization:

For circularly polarized light, the light vector rotates around the line of propagation, and its magnitude remains constant. Circularly polarized light may be resolved into components in any two directions at right angles. These components must always have the same amplitude.

Elliptical Polarization:

This is essentially similar to circular polarization except that the magnitude of the light vector changes periodically during the rotation. Elliptical polarization is seldom used in photo-elasticity.

Birefringence or Double Refraction:

Plates made of certain crystalline material, such as mica, have the property of resolving the light (which falls on them at normal incidence) into two components and transmitting it on planes at right angles. This phenomenon is referred to as "double refraction" or "birefringence". Furthermore, the optical properties on the two planes of transmission may be different so that the two components will be transmitted with different velocities. Therefore, when they emerge from the plate, there is a difference in phase between the two waves that is proportional to the thickness of the plate traversed by the light. Materials used in photo-elasticity must become birefringent when they are stressed.

Basic Optical Laws of Two-dimensional Photo-elasticity:

Almost all of the transparent materials such as glass, celluloid, bakelite, etc., become doubly refracting when subjected to deformations. There are two basic laws governing the relationship between the transmission of light and stresses:

(a) The light is polarized in the direction of principal-stress axes and is transmitted only on the planes of principal stress.

(b) The velocity of transmission in each principal plane is dependent on the magnitude of the principal stress in that plane.

Relative Retardation:

With an unstrained model of birefringent material, coated with reflective material on one side, any polarized light falling on it will be reflected back to the analyzer without any change. However, when the model is subjected to deformations due to external loading, the behavior of the polarized light will be governed by the above two laws. Plane polarized light will split into two perpendicular principal planes and the light in these planes will traverse the width of the model with different velocities. Thus, as these components progress through the model, they gradually become out of phase and emerge from the model at different times. The lag of one component over the other, as measured in inches is termed "relative retardation". The emerging components of light cannot be reunited to form a plane-polarized light again, so they reach the analyzer at different times. This effect appears in the form of different colors on the model as it is observed through the analyzer. The relative retardation (δ_n) depends directly on:

(a) the thickness of plastic (t_p) traversed by the light;

(b) the strain optical sensitivity constant (K) of the plastic;

(c) the principal strain difference ($\varepsilon_1-\varepsilon_2$).

These factors may be related as follows:

$$\delta_n = 2t_pKC(\varepsilon_1-\varepsilon_2). \qquad (2)$$

($2t_p$ is used since the light is reflected back. C is the reinforcing factor for the birefringent coating.)

The relative retardation, (δ_n), is measured in a photo-elastic experiment and, knowing the properties of the plastic, the value of the principal strain or stress difference can be calculated for a particular value of relative retardation. This is a constant value for a particular plastic.

Two types of fringe pattern are observed in a photostress experiment, isoclinics and isochromatics. An isoclinic at a point gives the direction of principal stresses at that point. The isochromatics give the principal stress difference at the point. Isochromatics appear as black and white fringes with a monochromatic source of light and appear as different colors with a white light source. The sequence of colors is shown in Fig. 1.

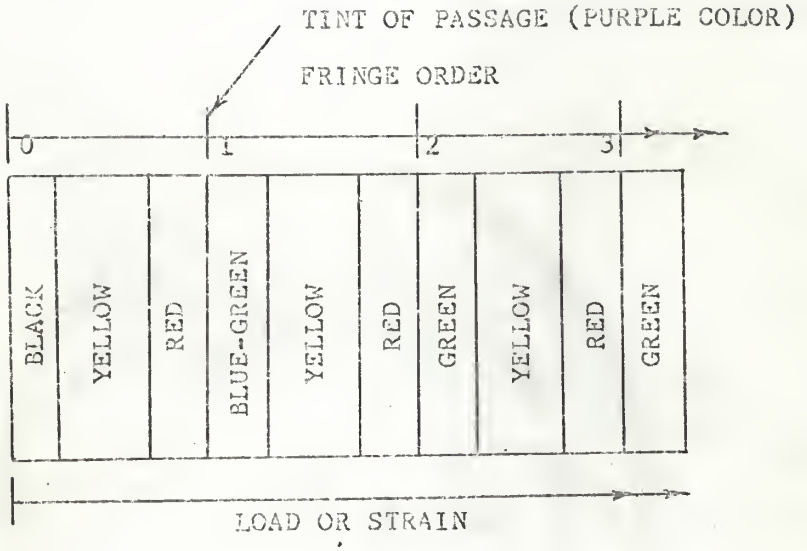

FIGURE 1. SKETCH SHOWING SEQUENCE OF COLORS WITH WHITE LIGHT SOURCE

EQUIPMENT

The Chapman Photo-elastic Model Making Kit:

This special model making kit was used to machine the photo-stress sheet to the required shape. A high speed vibrating jig saw was used to cut the sheet roughly to the required shape without putting pressure on the saw. An aluminum template, 0.100" thick, of the required shape was prepared very precisely and the rough plastic sheet was fixed to it so that about 1/16 inch of the plastic projected from the template all around. The plastic was then ready for rough finishing.

The finishing was done on a high speed model making machine which had a circular carbide cutter. For rough finishing a plug of slightly larger diameter than the diameter of the cutter was used. The plug projected exactly 0.100" above the base of the machine. For final finishing a second plug of the same diameter as that of the cutter was used. Very little pressure was applied to the template while guiding the plastic so as to avoid the generation of excessive heat in the plastic.

Polariscope:

A Large Field Meter with its accessories was used to make the photo-elastic observations. It consists of a polarizer and an analyzer arranged so that light from the polarizer falls on the model and is reflected back to the analyzer. The polarizer and the analyzer are coupled together so that they can be rotated simultaneously and the isoclinics of

different angles can be read on the isoclinic scale. The analyzer consists of an analyzer ring with a scale to measure the fractional fringe orders. The analyzer and the polarizer can be rotated together through 45^{o} angles either clockwise or counter-clockwise so as to produce plane or circularly polarized light. By producing circularly polarized light the isoclinic fringe pattern can be eliminated to facilitate the observation of isochromatics.

Preparation of Test Beam:

For experimental purposes an aluminum alloy 6061-T6 I-beam 5"x3" and 36" long was selected. A rectangular hole 2"x4" was cut in the middle of the beam with the corners of the hole rounded by 1/2 inch fillets. Photo-stress sheet plastic of type S was selected and was machined to the required shape. The plastic was then applied to the web of the beam as shown in Figs. 2a and 2b. Photo-stress RCT (S&A) reflective cement resin and hardener were used to fasten the plastic sheet to the beam web. The cement was applied in a uniformly thin layer of about 1/32 inch thickness and care was taken to prevent air bubbles. The bonding was allowed to harden for a minimum of 24 hours.

The electric-resistance strain gages were then mounted at the selected places as shown in Figs. 3a through 3d. Eastman 910 contact cement was used for bonding the gages to the beam.

Loading Arrangement:

The load was applied at the center of the beam through a steel block 1"x1"x2" which was placed longitudinally on the center line of the flange. A hydraulic testing machine was used to apply the load. The beam was aligned as perfectly as possible over the supports so as to avoid any twisting in it. A compression load cell was used to measure the load accurately. The general arrangement of the setup is shown in Fig. 4.

Strain Gage Indicator and Accessories:

The strain gages were connected to a Digital Strain Indicator (Budd Model A110) which was further connected to a Strain Gage Switch and Balance Unit (Budd Model C-10T and C-10LTC). The strain gages were balanced for zero load with the aid of this unit. The strain gage readings were recorded with the help of an Automatic Printer.

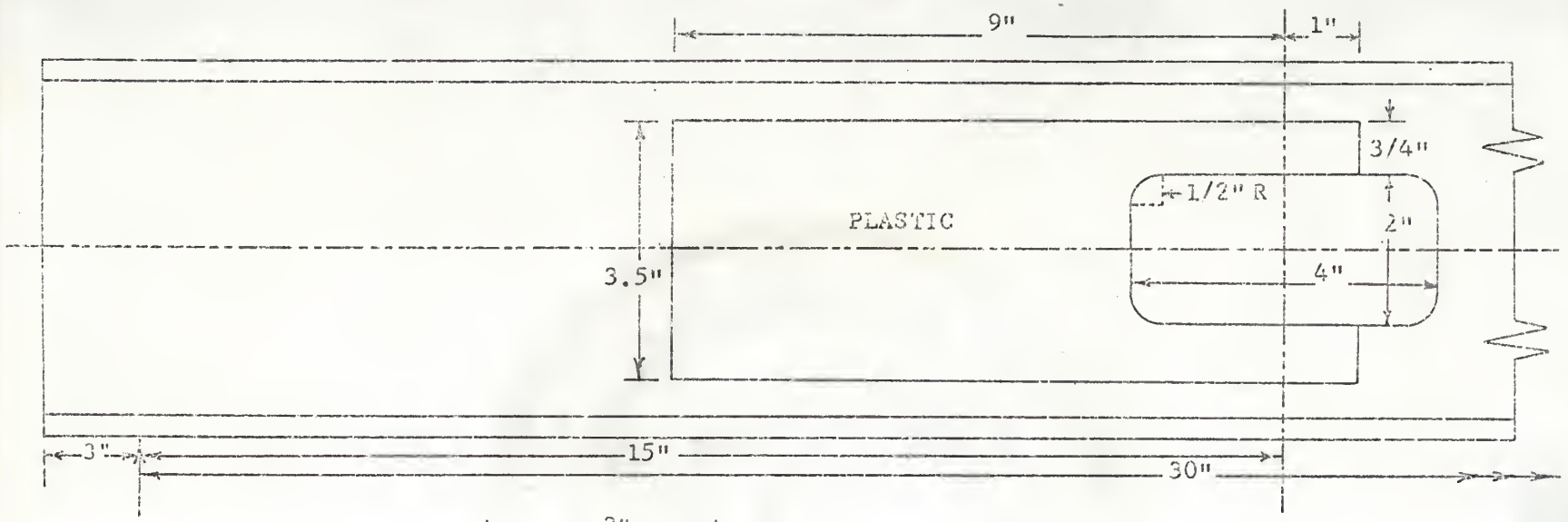

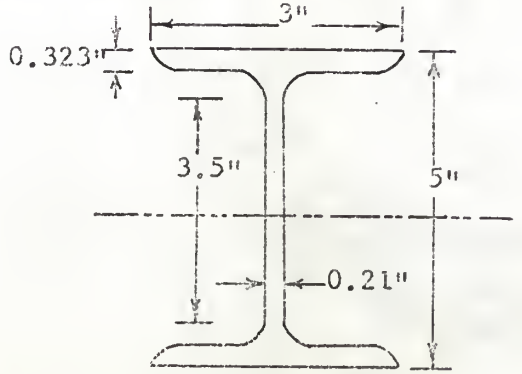

X - SECTION OF THE BEAM
5" x 3" @ 3.43

AREA = 2.92 in.^{2},
I = 12.26 in.^{4},
S = 4.90 in.^{3},
E_s = 10 x 10^6 psi,
μ_s = 0.33.

FIGURE 2a. BEAM SHOWING LOCATION OF PHOTOSTRESS PLASTIC

FIGURE 2b. PHOTOGRAPH OF THE BEAM WITH PHOTOSTRESS PLASTIC CEMENTED TO THE WEB

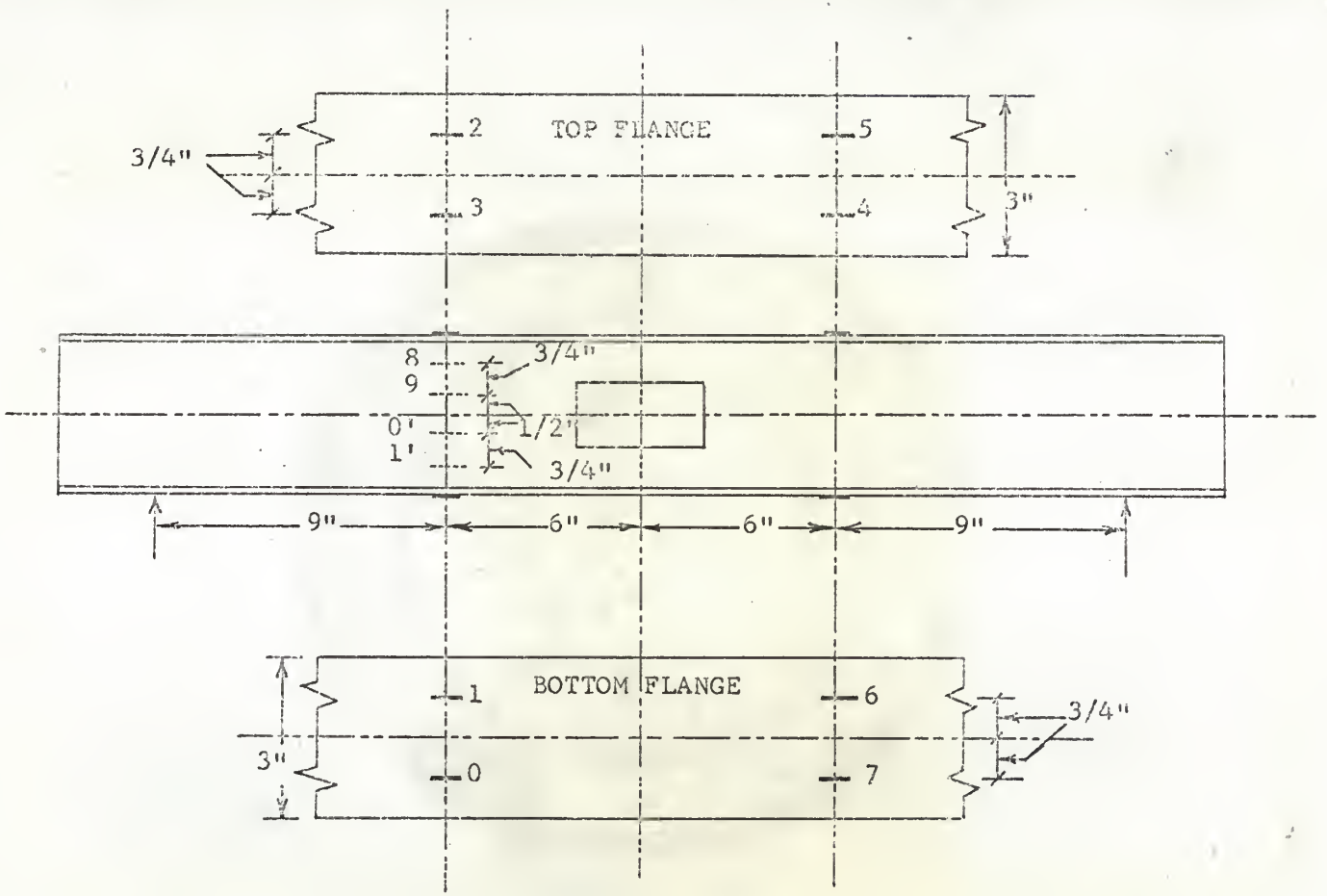

FIGURE 3a. ARRANGEMENT OF THE STRAIN GAGES

FIGURE 3b. PHOTOGRAPH OF THE FLANGE SHOWING STRAIN GAGES 0, 1, 6 AND 7

FIGURE 3c. PHOTOGRAPH OF THE FLANGE SHOWING STRAIN GAGES 2, 3, 4, AND 5

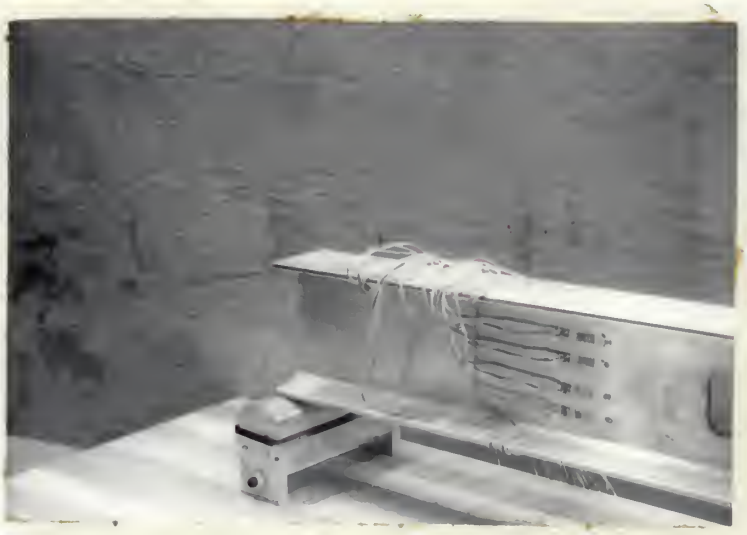

FIGURE 3d. PHOTOGRAPH OF THE WEB SHOWING STRAIN GAGES 8, 9, 0' and 1'

FIGURE 4. PHOTOGRAPH OF THE GENERAL SETUP OF THE EXPERIMENT

Fringe Value: (f)

The fringe value may be defined as the magnitude of principal strain difference $(\varepsilon_1-\varepsilon_2)$ or principal stress difference $(\sigma_1-\sigma_2)$ required to produce one fringe in the photo-stress plastic.

It can be seen from equation (2) that relative retardation $\delta_n = 2t_pKC(\varepsilon_1-\varepsilon_2)$. Also, fringe order $N_n = \delta_n/\lambda$, where λ is the wave length of light corresponding to the retardation at the tint of passage. So,

$$(\varepsilon_1-\varepsilon_2) = \lambda N_n/(2t_pKC) \qquad (3)$$

Photostress sheet plastic of type S was used. Since in this case there was no bending in the plane of plastic, the reinforcing factor, C, was neglected.

From equation (3), fringe value $f = \lambda/(2t_pK)$, $(N_n = 1)$. (4)

For the type of plastic used:

$t_p = 0.120"$,

$K = 0.084$,

and $\lambda = 22.7 \times 10^{-6}$ inches.

Therefore, from equation (4):

$f = (22.7 \times 10^{-6})/(2\times0.12\times0.084)$,

$= 1.125 \times 10^{-3}$ inches/inch,

$= 1125$ micro-inches/inch.

Converting this into principal stress difference $(\sigma_1-\sigma_2)$,

$$(\sigma_1-\sigma_2) = (\varepsilon_1-\varepsilon_2)E_s/(1+\mu_s). \qquad (5)$$

E_s, the modulus of elasticity of the structure; i.e., aluminum alloy 6061-T6, is approximately 10×10^6 psi. (13)

μ_s, the Poisson's ratio of the structure; i.e., aluminum alloy 6061-T6, is approximately 0.333. (13)

Therefore, from equation (5):

$$(\sigma_1-\sigma_2) = 1125 \times 10^{-6} \times (10 \times 10^6)/(1+0.333) \text{ psi},$$

$$= 11250/1.333 \text{ psi},$$

$$= 8420 \text{ psi}.$$

In other words, 8420 psi. principal stress difference is required to produce one fringe of birefringence in this type of plastic when cemented to aluminum alloy 6061-T6.

Calibration of Full Wave Plate:

Since sufficient load could not be applied (due to the presence of the hole) to develop a full fringe or more at most of the points on the plastic, it was necessary to use the compensator and the full wave plate to observe the birefringence between zero and the first fringe. A full wave plate should add exactly one fringe at all the points but most of the time these plates have some initial errors. Therefore, they should be calibrated. The following calibration procedure was used:

The uncoated reflective surface was observed through the analyzer with the full wave plate mounted on it. The analyzer ring was rotated clockwise or counter-clockwise to observe the tint of passage (purple color). The tint of passage in the present case occurred at a 0.09 reading with counter-clockwise rotation of the analyzer ring. Hence all of the observations made with the aid of the full wave plate

were increased by 0.09.

Photostress Observations:

For the purpose of making photostress observations, the Large Field Meter was set up at a distance of about two feet from the beam. Initial adjustments were made to remove parasitic reflections. A particular grid pattern (shown in Fig. 5) was selected on the plastic to make point by point observations. With the polariscope producing plane polarized light, the analyzer handle was rotated clockwise or counter-clockwise to bring an isoclinic to the particular point of interest. The polariscope was then adjusted to produce circularly polarized light so that the isoclinics were eliminated. The full wave plate and the compensator were then mounted on the analyzer. The compensator was used to determine between which two fringes the point of interest lay. The full wave plate and the compensator are additive only when the analyzer handle is parallel to the direction of major principal stress (14a). With the compensator parallel to the direction of the major principal stress, the zero fringe should appear. Thus the compensator was used to observe whether or not the zero fringe appeared. If the zero fringe appeared, the analyzer handle was parallel to the major principal stress otherwise it was not. The analyzer handle was rotated clockwise or counter-clockwise through 90° from its original position if it was not parallel to the major principal stress. Hence, in all observations made with the aid of the full-wave plate, the analyzer handle was kept

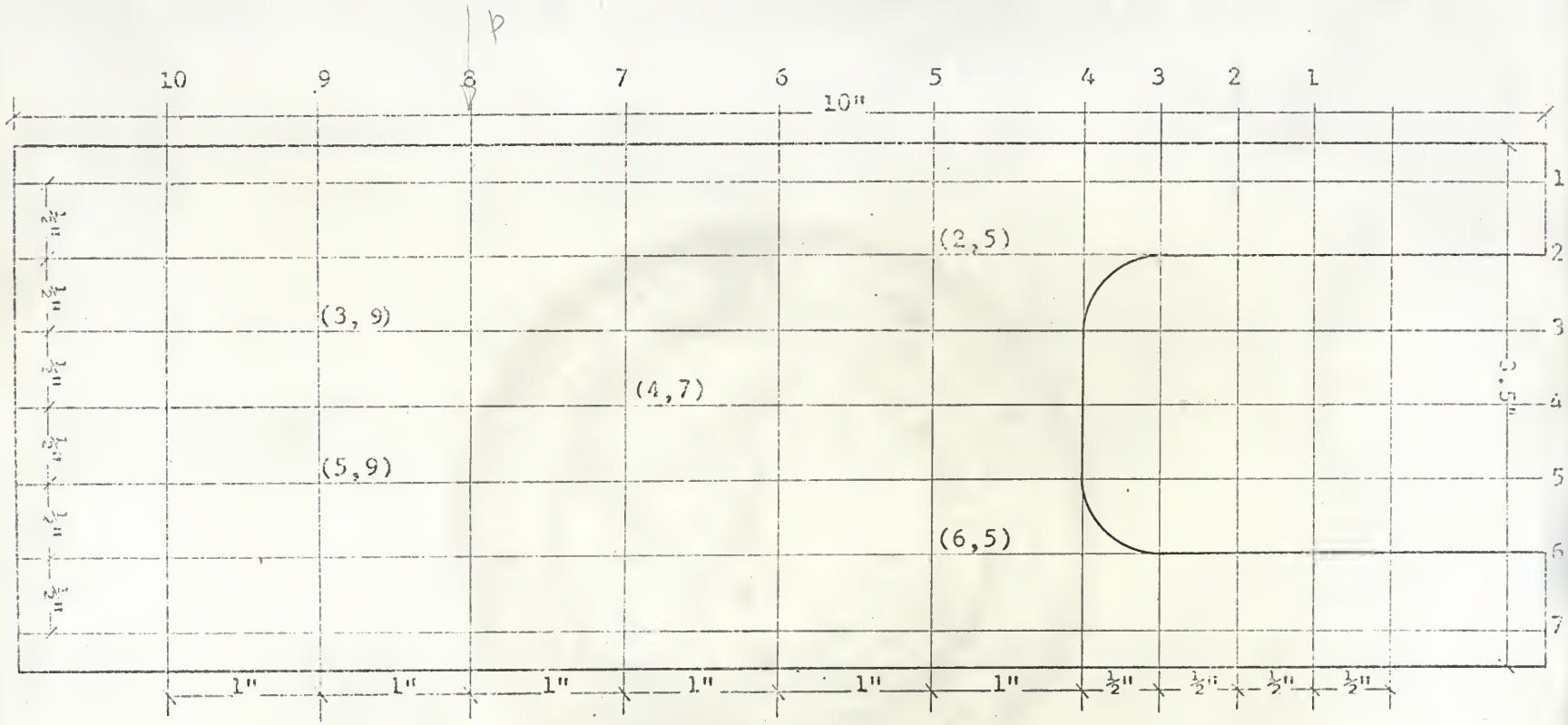

FIGURE 5. SKETCH SHOWING GRID PATTERN ON THE PLASTIC

parallel to the direction of major principal stress and the analyzer ring always required clockwise rotation to bring the lower fringe on to the point of interest.

The observations were made for four different increments of load. The values of the isoclinics and the isochromatics are shown in Figs. 6 to 9. The beam was then reversed from end to end; i.e., the plastic was on the right side of the beam and the compression flange was in tension. The photostress observations were again taken with the beam in the second position. The values of the isoclinics and the isochromatics, for 4000 lbs. load at the center, for this position of the beam are shown in Fig. 10. Some of the isoclinic and isochromatic photographs are shown in Figs. 11, 12 and 13.

Strain Gage Readings:

The strain gage readings were also recorded for four different loads. These readings are shown in Table 1. With the beam reversed, the strain gage readings for four increasing load conditions were again recorded and these are shown in Table 2.

The photostress observations and the strain gage readings for the two positions of the beam agreed quite well. The calculations were done for the first position of the beam; i.e., with the plastic on the left side of the beam.

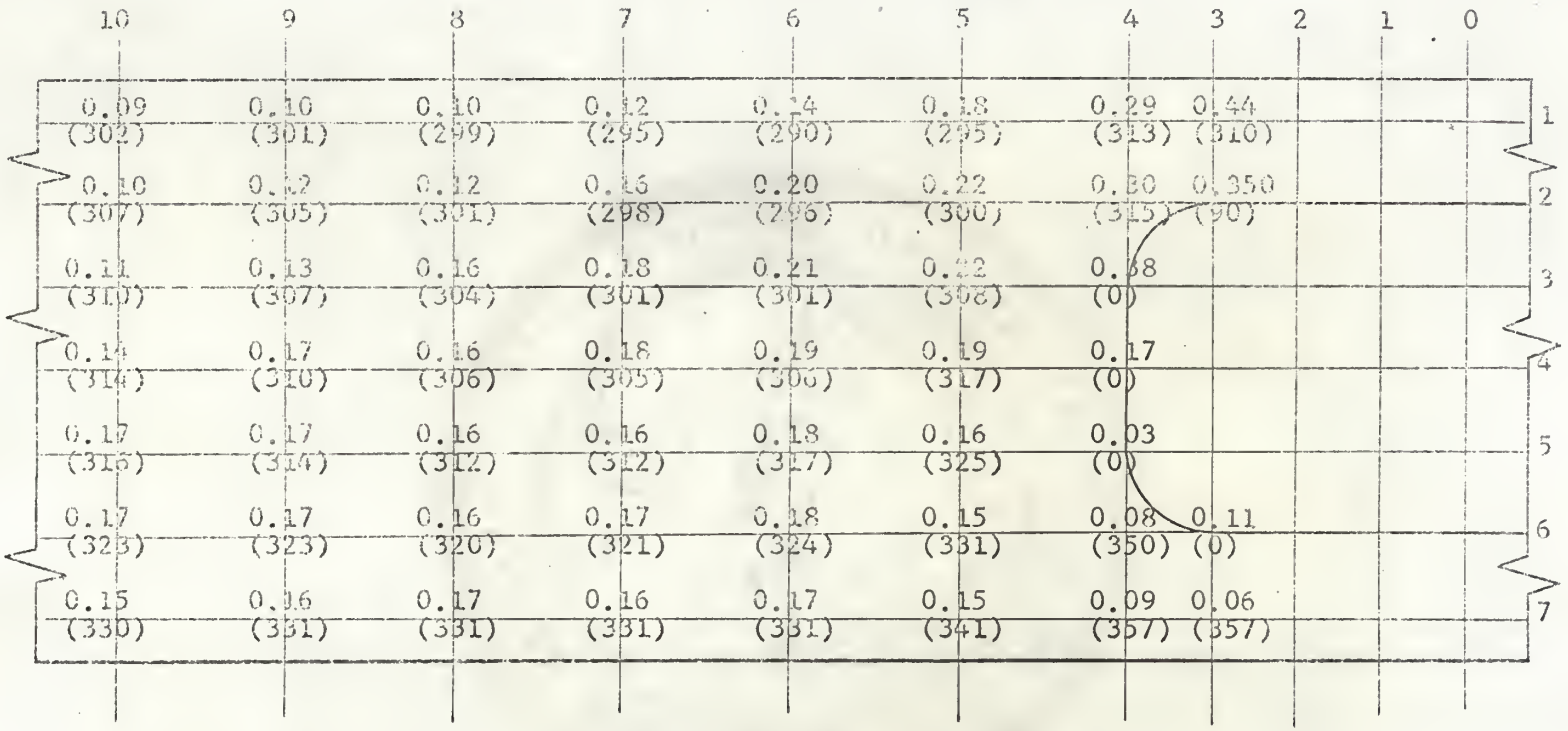

FIGURE 6. ISOCLINIC ANGLES (IN PARENTHESES) AND ISOCHROMATIC READINGS FOR 1210 LBS. LOAD (PLASTIC ON THE LEFT SIDE)

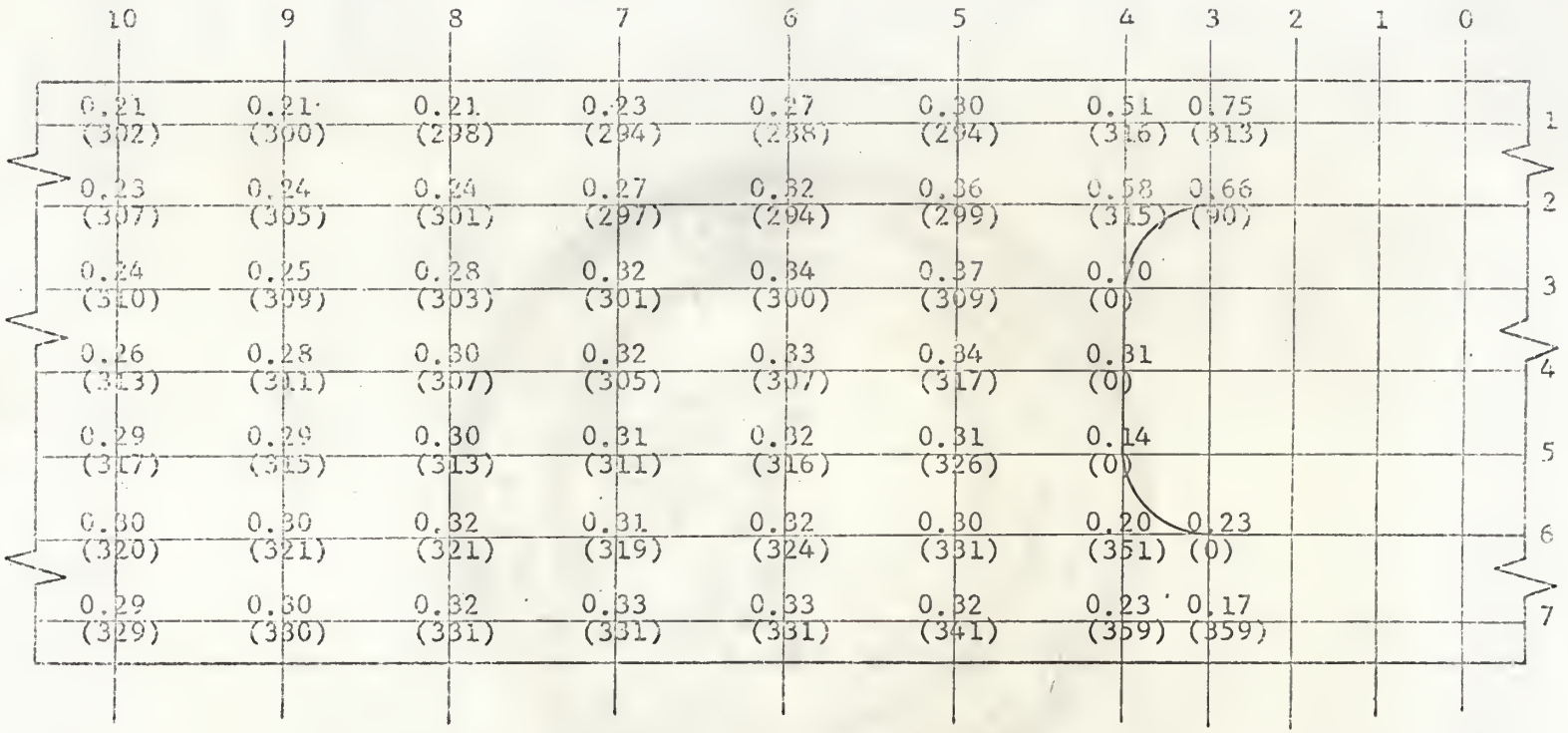

FIGURE 7. ISOCLINIC ANGLES (IN PARENTHESES) AND ISOCHROMATIC READINGS FOR 2060 LBS. LOAD (PLASTIC ON THE LEFT SIDE)

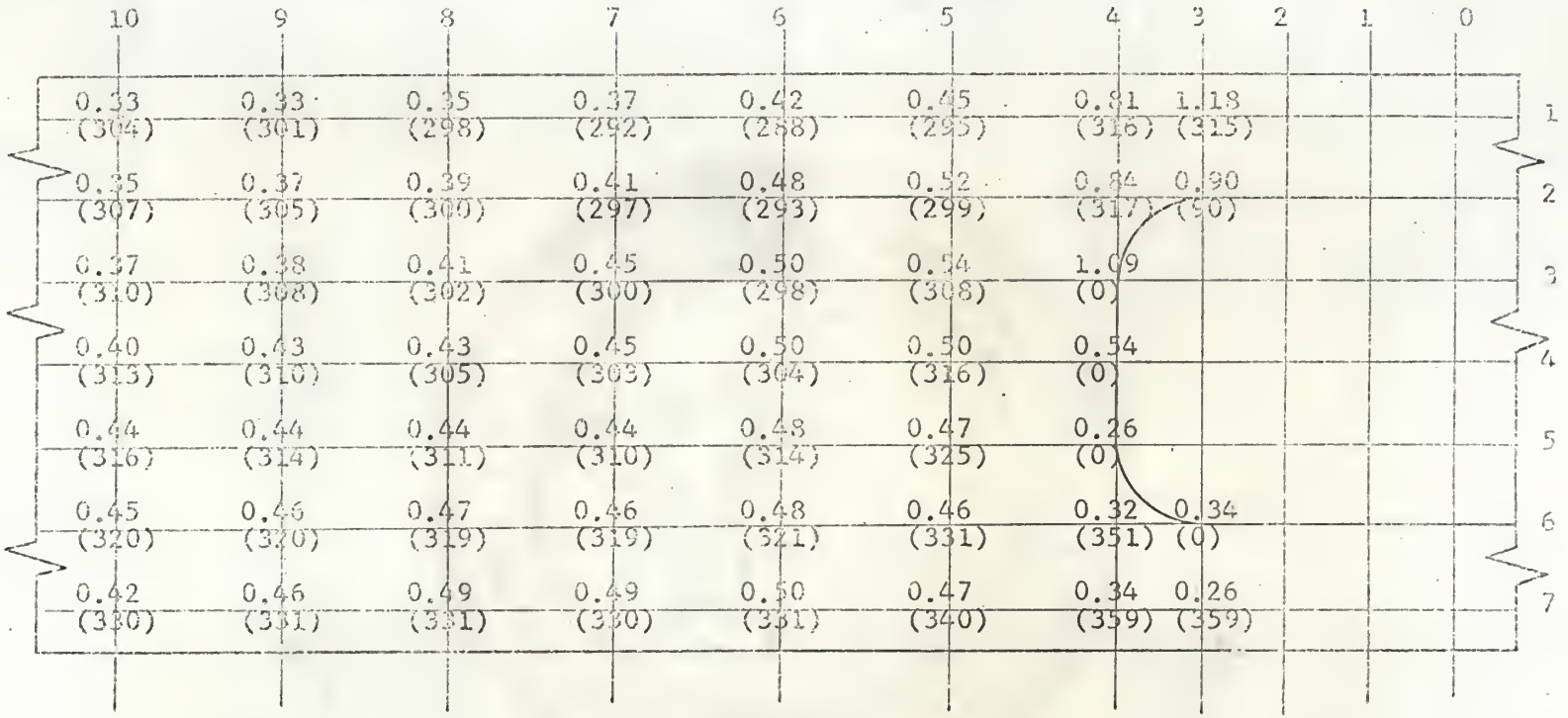

FIGURE 8. ISOCLINIC ANGLES (IN PARENTHESES) AND ISOCHROMATIC READINGS FOR 3035 LBS. LOAD (PLASTIC ON THE LEFT SIDE)

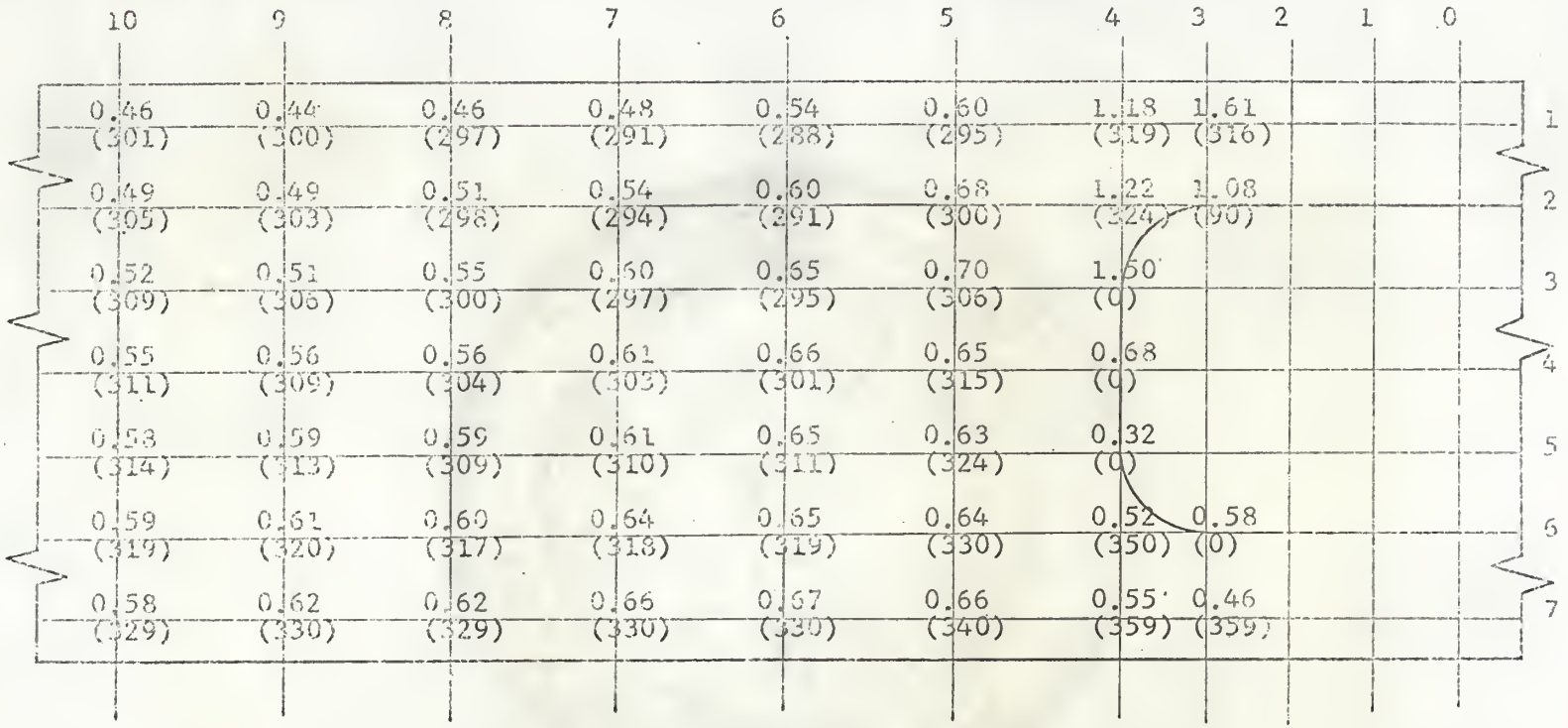

FIGURE 9. ISOCLINIC ANGLES (IN PARENTHESES) AND ISOCHROMATIC READINGS FOR 4105 LBS. LOAD (PLASTIC ON THE LEFT SIDE)

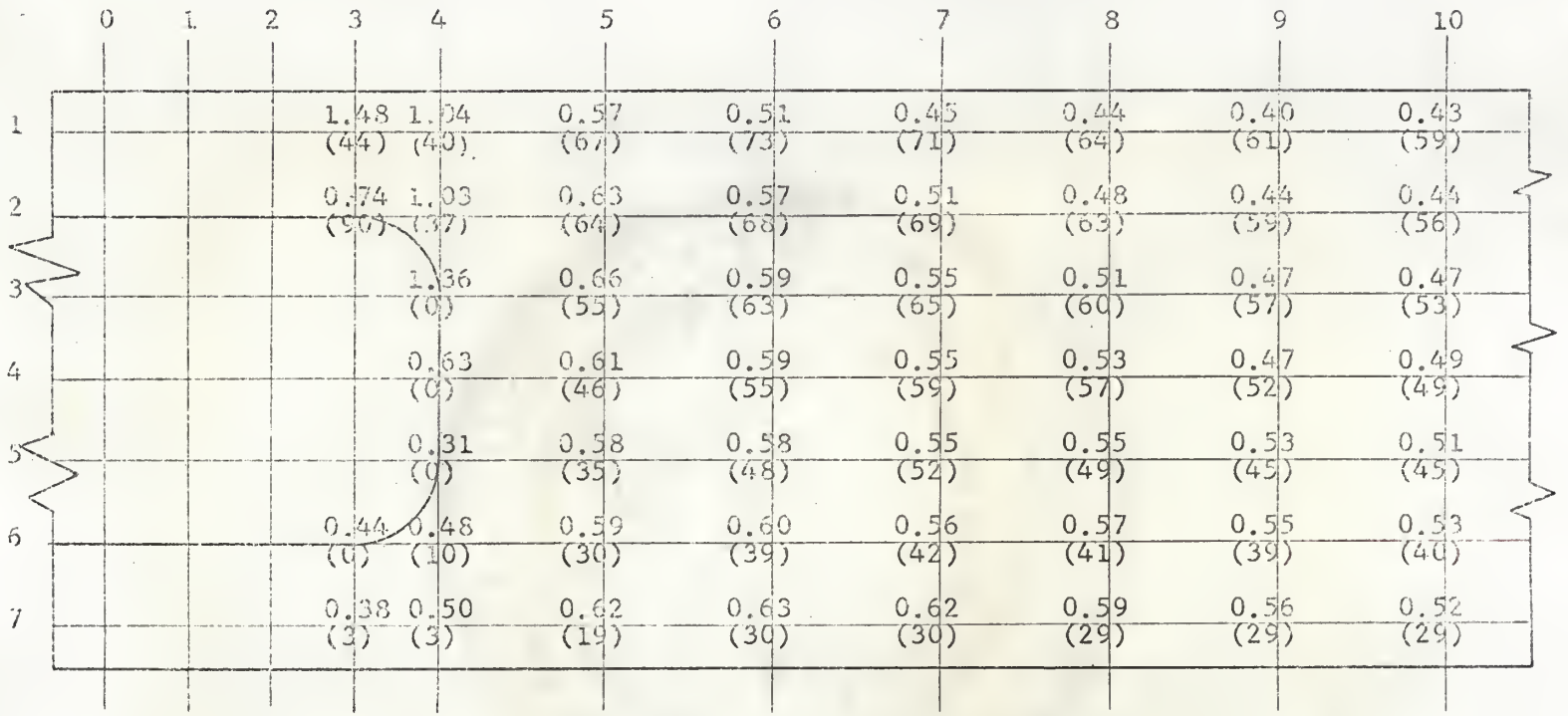

FIGURE 10. ISOCLINIC ANGLES (IN PARENTHESES) AND ISOCHROMATIC READINGS FOR 4000 LBS. LOAD (PLASTIC ON THE RIGHT SIDE)

FIGURE 11a. FRINGE PHOTOGRAPH WITH THE PLASTIC ON THE LEFT SIDE (LOAD = 4100 LBS.)

FIGURE 11b. FRINGE PHOTOGRAPH WITH THE PLASTIC ON THE RIGHT SIDE (LOAD = 4100 LBS.)

FIGURE 12a. PHOTOGRAPH OF 60° ISOCLINIC WITH THE PLASTIC ON THE LEFT SIDE (LOAD = 4100 LBS.)

FIGURE 12b. PHOTOGRAPH OF 30° ISOCLINIC WITH THE PLASTIC ON THE RIGHT SIDE (LOAD = 4100 LBS.)

FIGURE 13a. PHOTOGRAPH OF 45° ISOCLINIC WITH THE PLASTIC ON THE LEFT SIDE (LOAD = 4100 LBS.)

FIGURE 13b. PHOTOGRAPH OF 45° ISOCLINIC WITH THE PLASTIC ON THE RIGHT SIDE (LOAD = 4100 LBS.)

TABLE 1. STRAIN GAGE READINGS WITH THE PLASTIC ON THE LEFT SIDE

STRAIN GAGE NO.	STRAIN GAGE READING IN MICRO-INCHES AT			
	1210 LBS.	2060 LBS.	3035 LBS.	4105 LBS.
0	+127	+214	+314	+423
1	+121	+212	+312	+422
2	-103	-183	-276	-373
3	-119	-198	-289	-387
4	-110	-189	-281	-378
5	-103	-181	-270	-366
6	+125	+211	+311	+422
7	+121	+208	+310	+422
8	- 75	-127	-188	-252
9	- 49	- 83	-122	-163
0'	+ 3	+ 5	+ 8	+ 12
1'	+ 50	+ 86	+127	+171

TABLE 2. STRAIN GAGE READINGS WITH THE PLASTIC ON THE RIGHT SIDE

STRAIN GAGE NO.	STRAIN GAGE READING IN MICRO-INCHES AT			
	1235 LBS.	2145 LBS.	3135 LBS.	4075 LBS.
0	-122	-209	-303	-393
1	-106	-185	-278	-352
2	+129	+228	+334	+434
3	+126	+219	+318	+414
4	+126	+223	+327	+425
5	+129	+223	+329	+427
6	-112	-193	-282	-365
7	-120	-208	-303	-394
8	+ 49	+ 85	+127	+162
9	+ 4	+ 7	+ 10	+ 13
0'	- 49	- 84	-122	-157
1'	- 76	-135	-195	-253

INITIAL CORRECTION OF RAW DATA

Since some initial or residual birefringence was present in the plastic, a zero load correction was necessary. It was observed that the birefringence reading (residual) at all the points was less than 0.10 of a fringe. It was further noted that with the increase of load, the isoclinic readings did not change much (the maximum variation being 3^{o} at a very few points)(Fig. 14). Therefore it was possible to add or subtract, directly, the zero load readings to obtain corrected readings. The photostress readings at each point, for four different loads were taken. A straight line graph was then drawn through the four readings for each point. If that straight line passed through the origin for a particular point, there was no residual birefringence at that point otherwise a parallel straight line was drawn through the origin to correct for the initial birefringence. Some of these graphs are shown in Figs. 15 through 19. The isoclinic angles for each point, at different loads, were also noted and the average of these angles were used in the calculations.

The straight line graph for four strain gage readings, at different loadings, for all of the strain gages were also drawn and some of these are shown in Figs. 20 through 27. Since the calculations were made for the 4000 lbs. load at the center (with the plastic on left side of the beam), the corrected interpolated birefringence readings and isoclinic angles for that load are shown in Fig. 28. The interpolated strain gage readings for 4000 lbs. load are shown in Table 3.

FIGURE 14a. FRINGE PHOTOGRAPH FOR ZERO LOAD

FIGURE 14b. PHOTOGRAPH OF 50° ISOCLINIC FOR ZERO LOAD

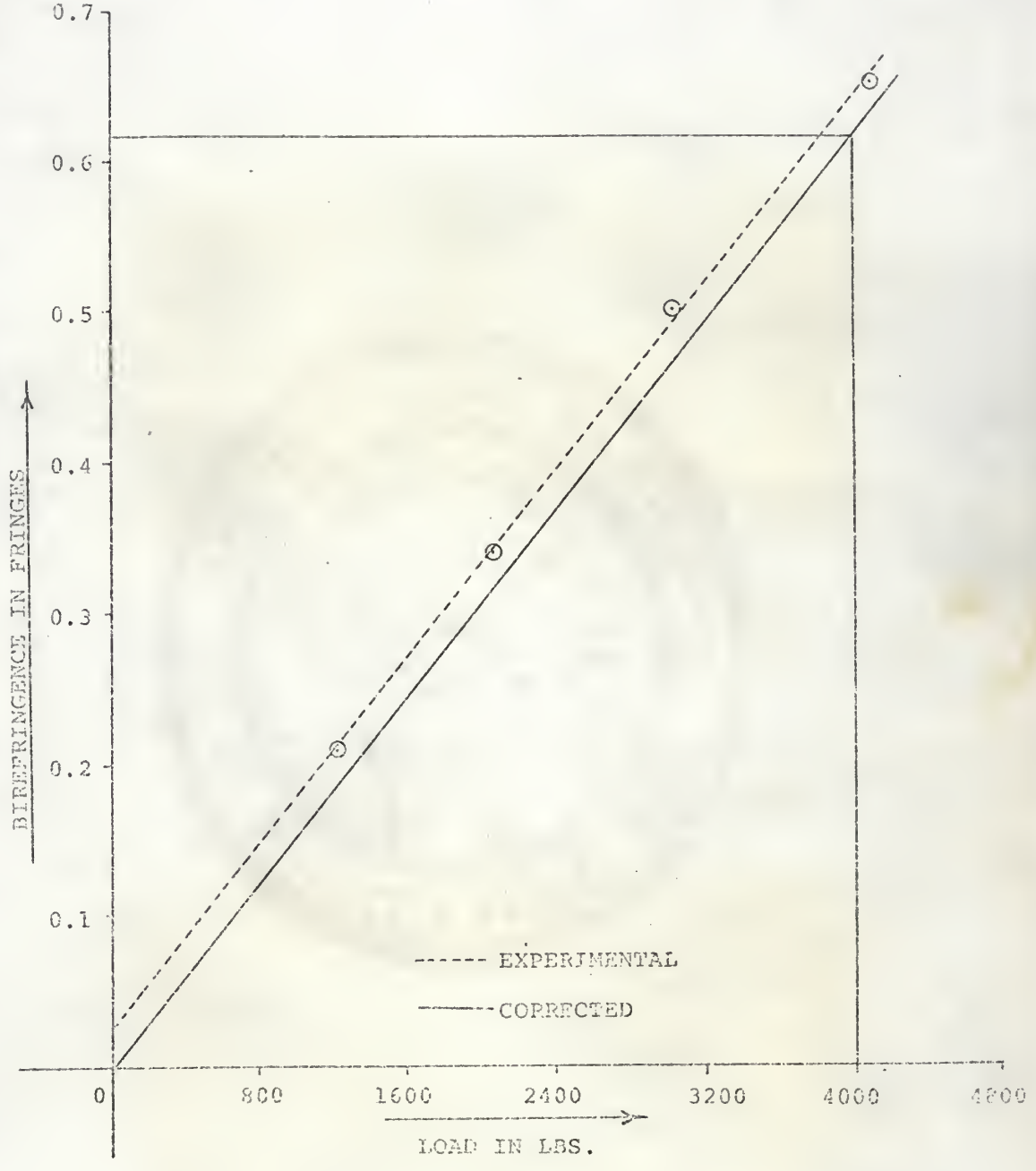

FIGURE 15. CORRECTION FOR RESIDUAL BIREFRINGENCE AT POINT (3,6)

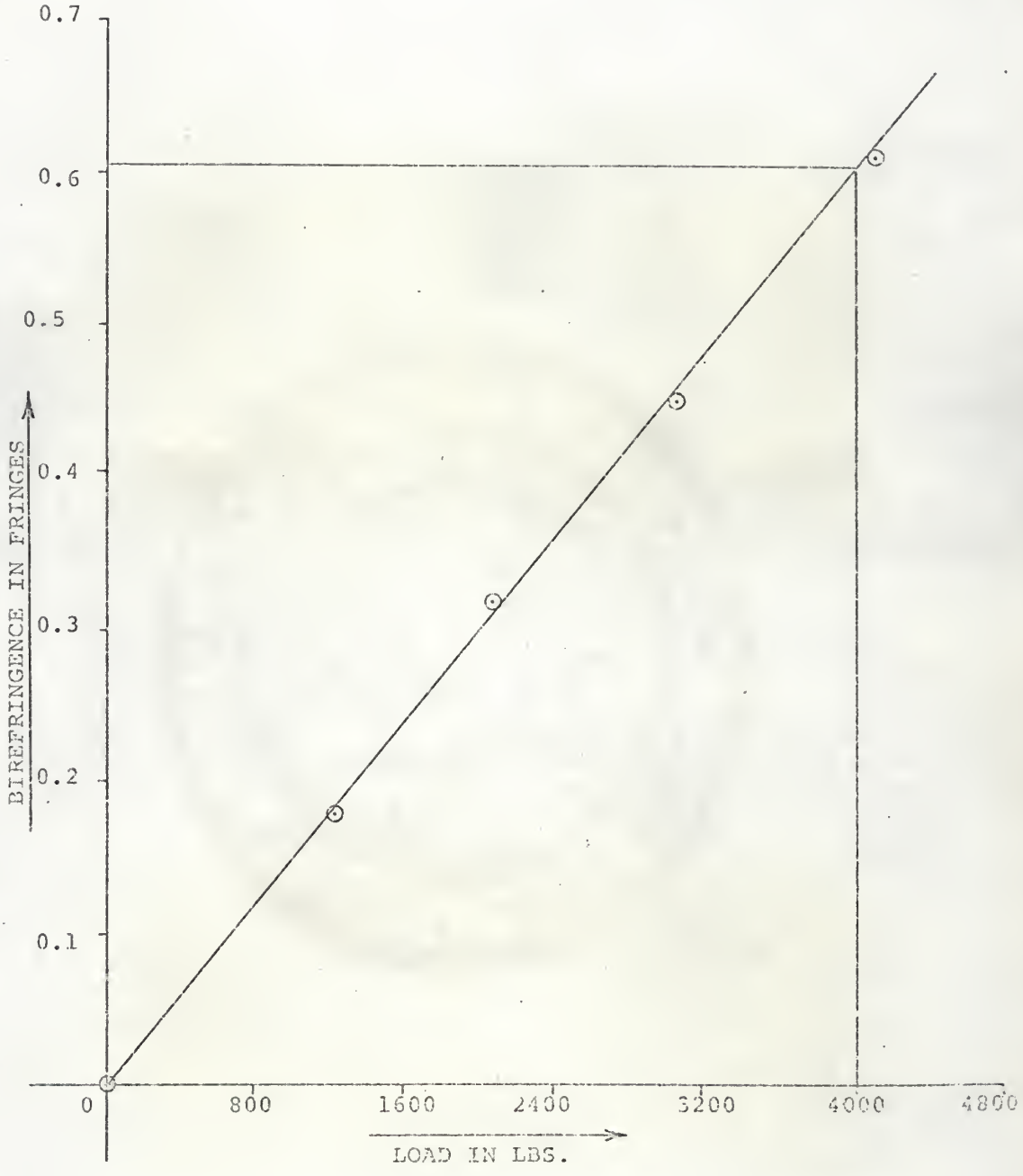

FIGURE 16. CORRECTION FOR RESIDUAL BIREFRINGENCE AT POINT (4,7)

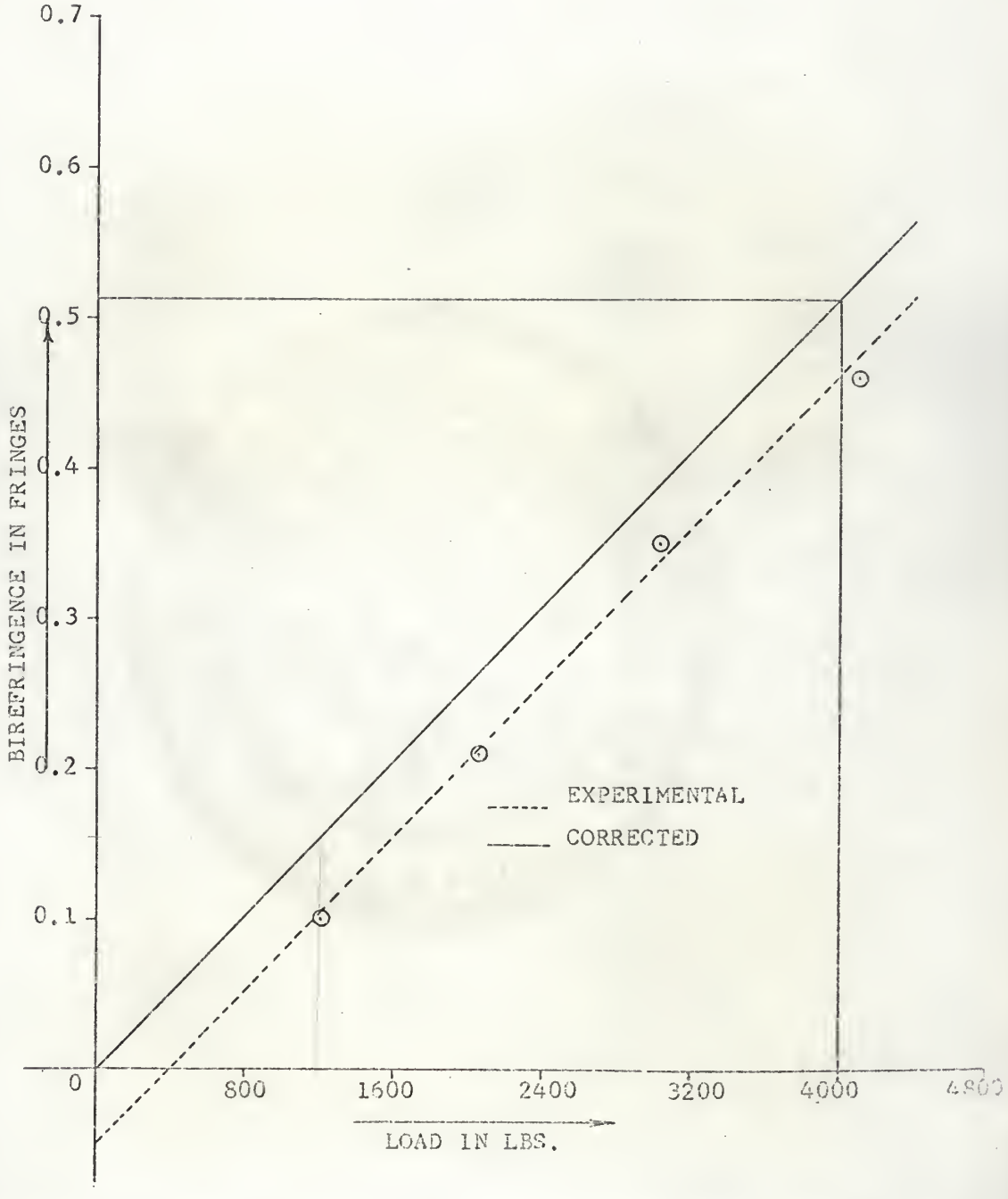

FIGURE 17. CORRECTION FOR RESIDUAL BIREFRINGENCE AT POINT (1,8)

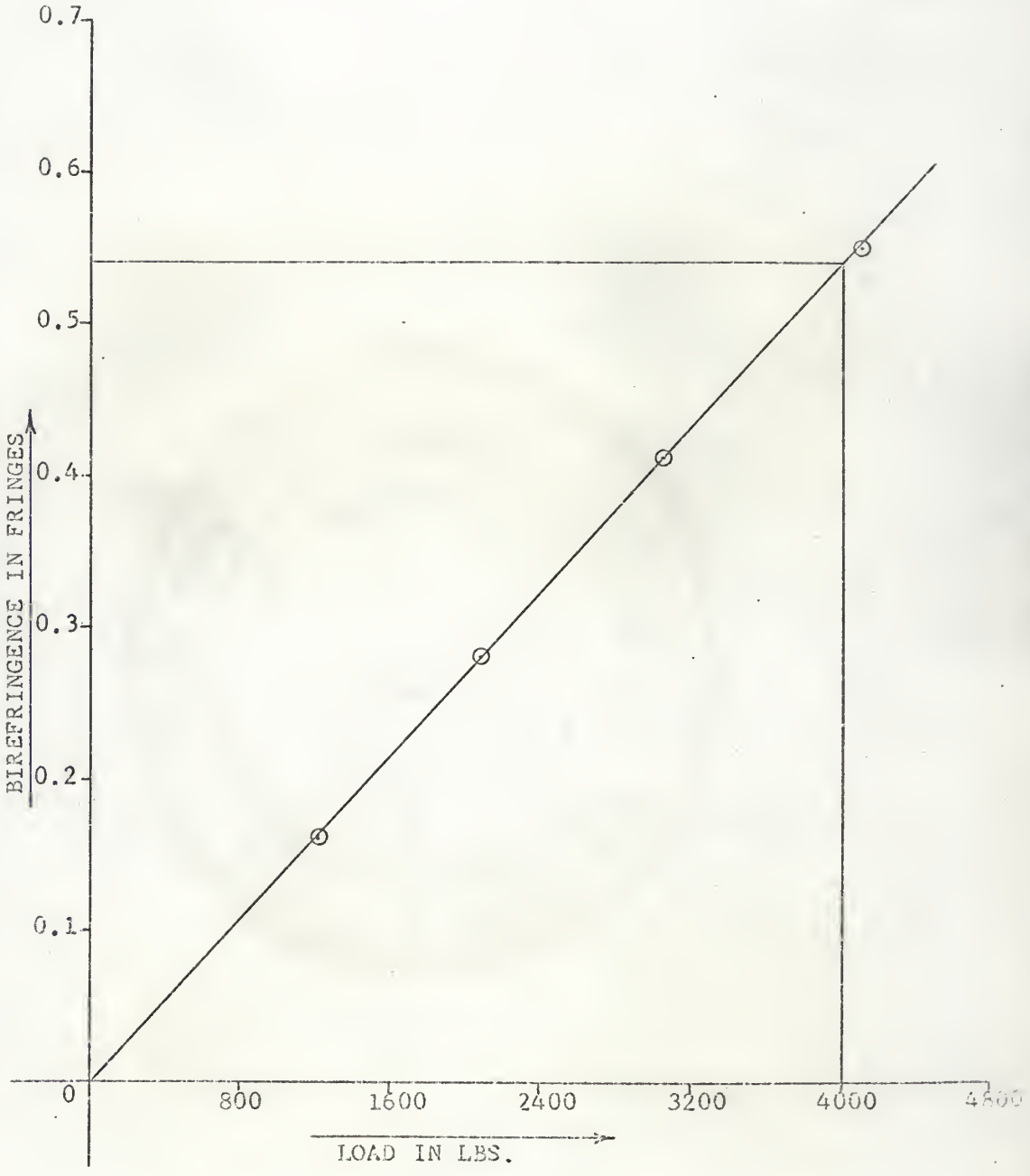

FIGURE 18. CORRECTION FOR RESIDUAL BIREFRINGENCE AT POINT (3,8)

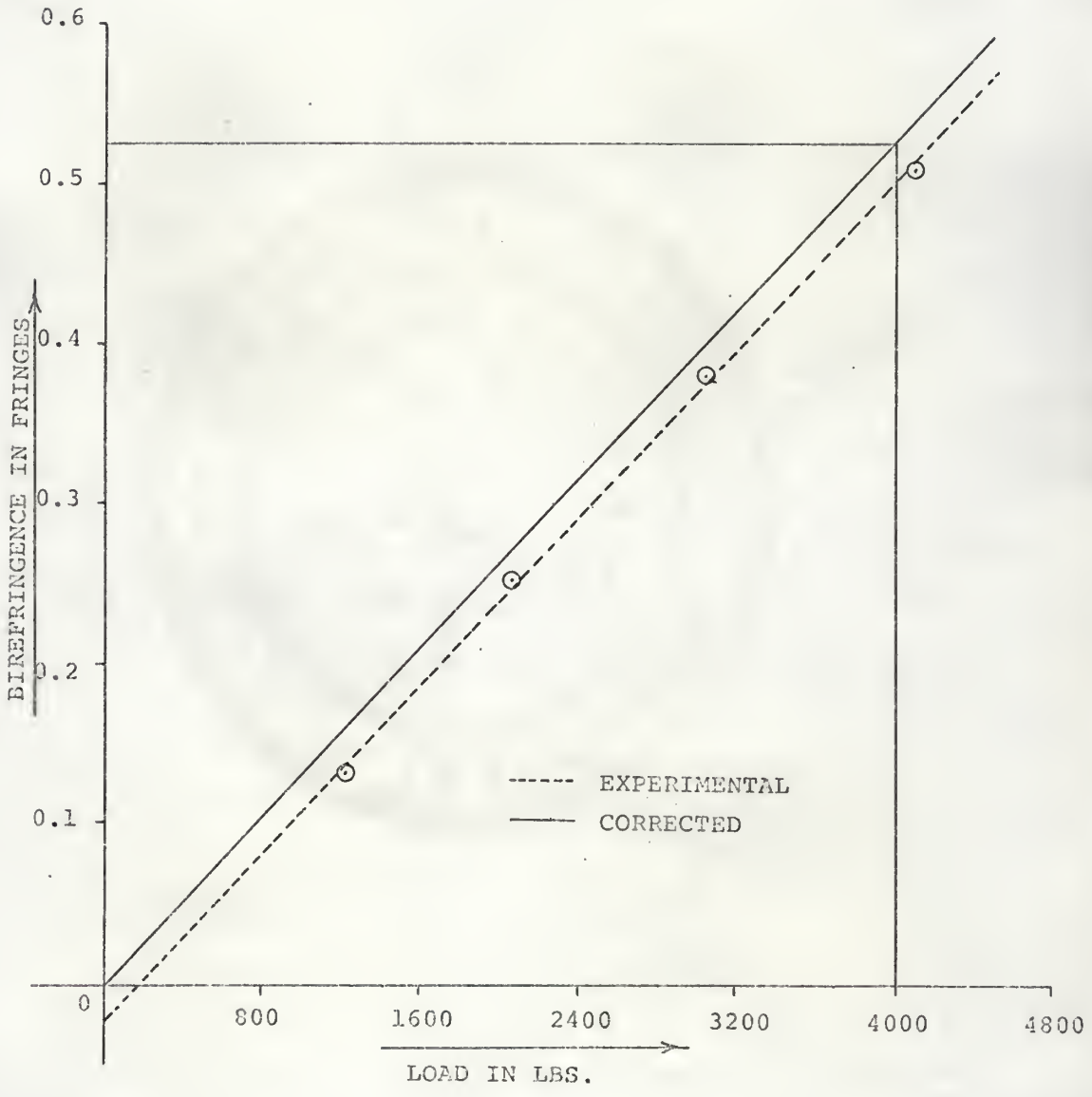

FIGURE 19. CORRECTION FOR RESIDUAL BIREFRINGENCE AT POINT (3,9)

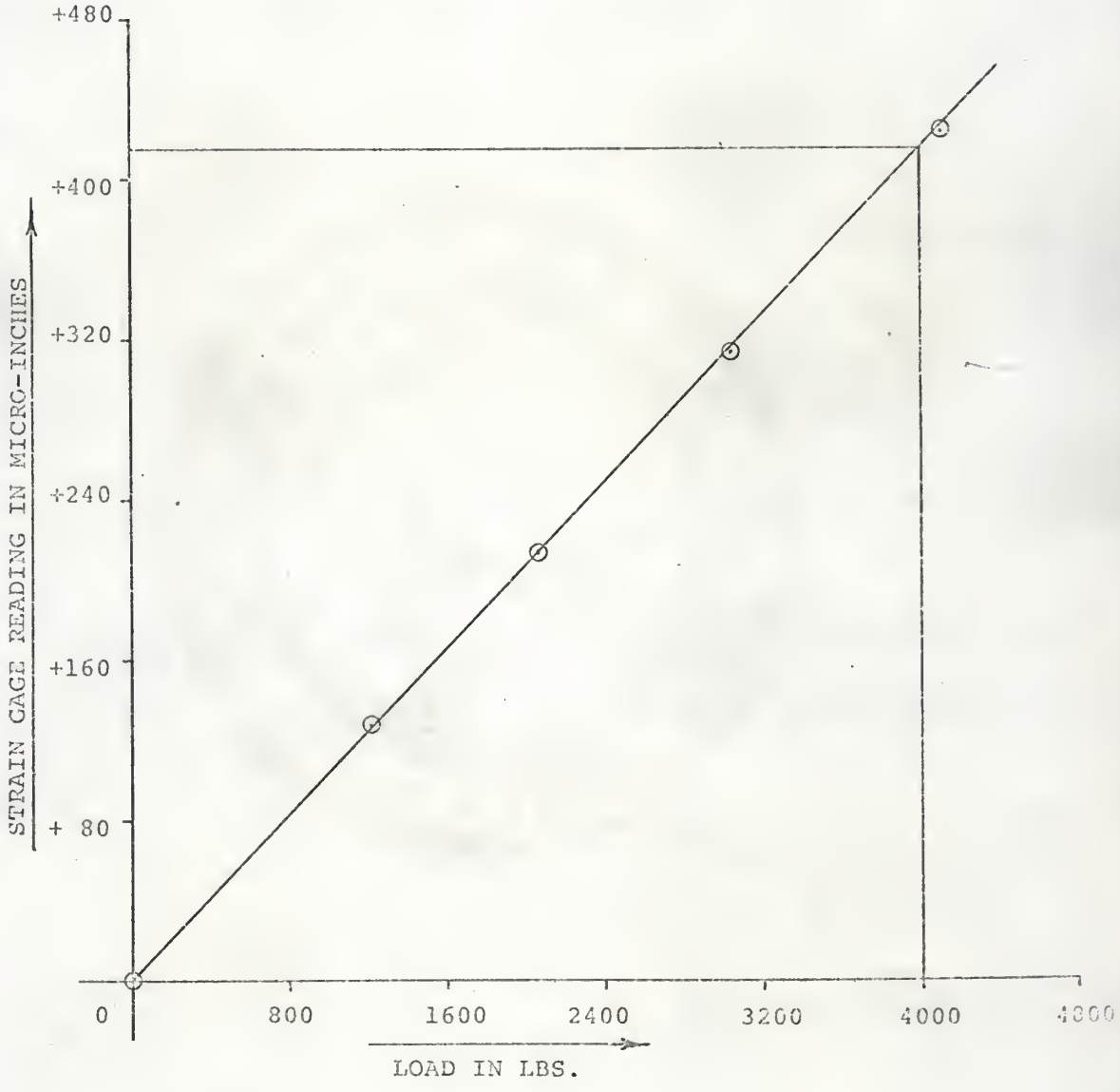

FIGURE 20. STRAIN GAGE READINGS FOR STRAIN GAGE NO. 0 AT FOUR LOAD LEVELS

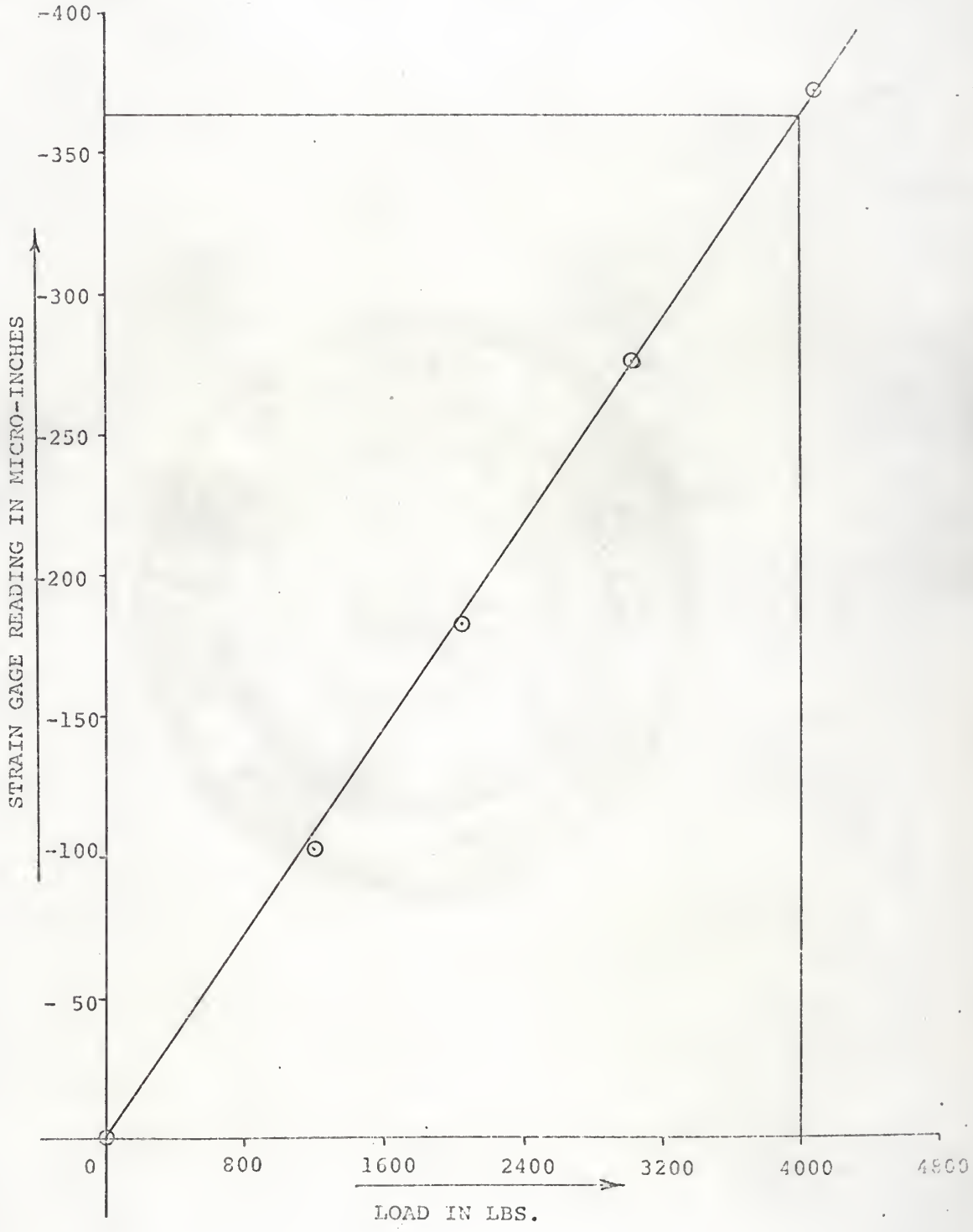

FIGURE 21. STRAIN GAGE READINGS FOR STRAIN GAGE NO. 2 AT FOUR LOAD LEVELS

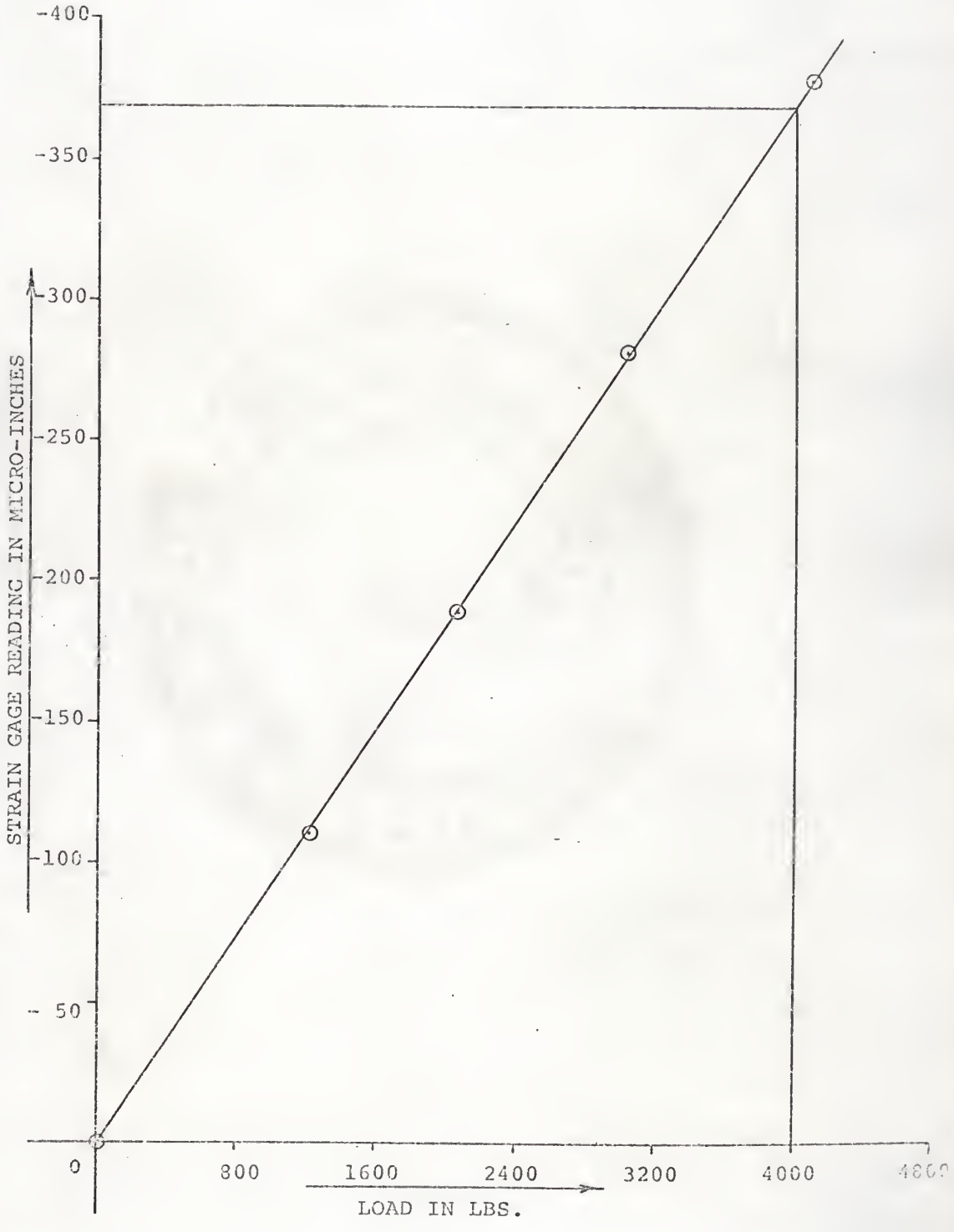

FIGURE 22. STRAIN GAGE READINGS FOR STRAIN GAGE NO. 4 AT FOUR LOAD LEVELS

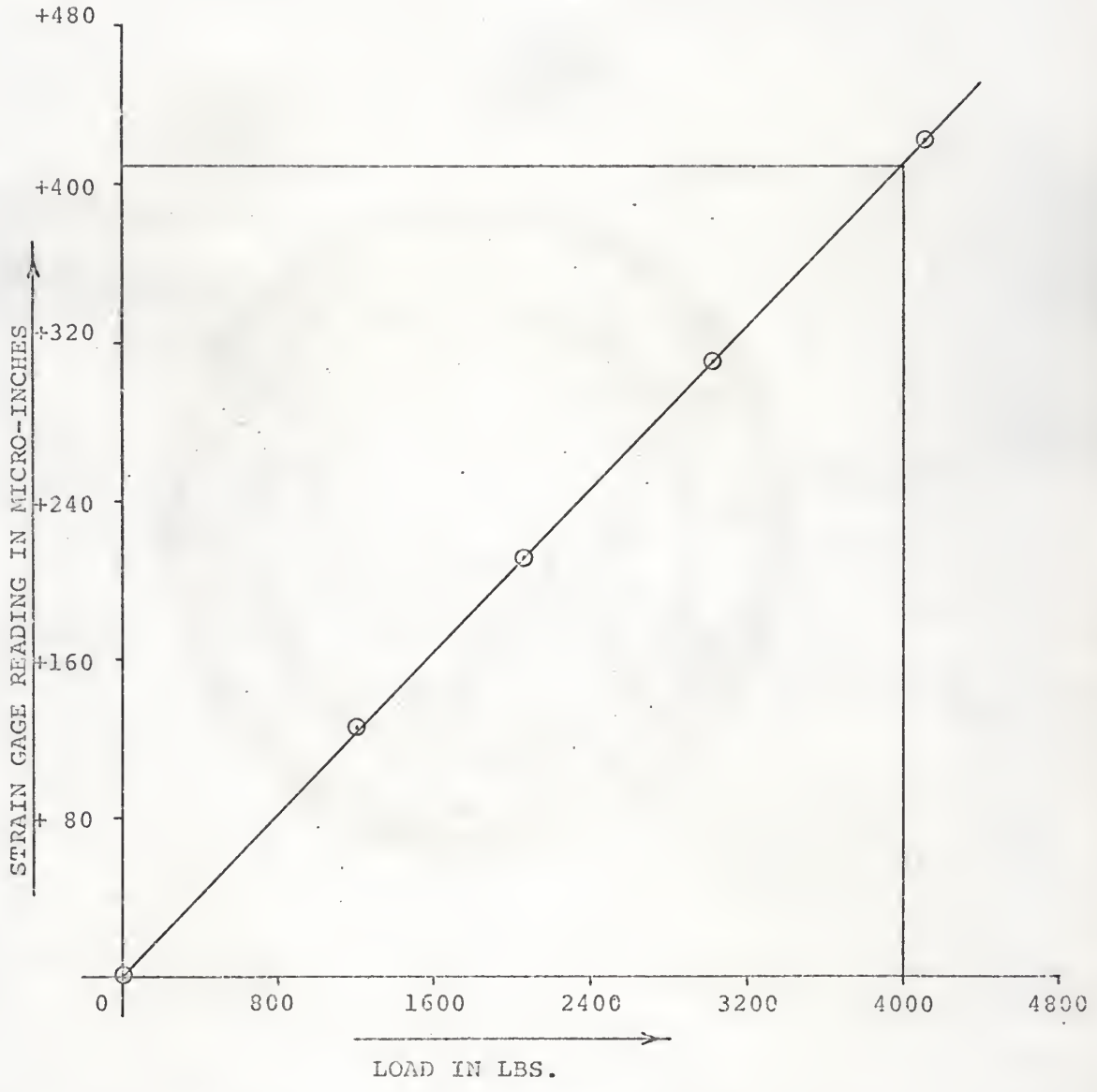

FIGURE 23. STRAIN GAGE READINGS FOR STRAIN GAGE NO. 6 AT FOUR LOAD LEVELS

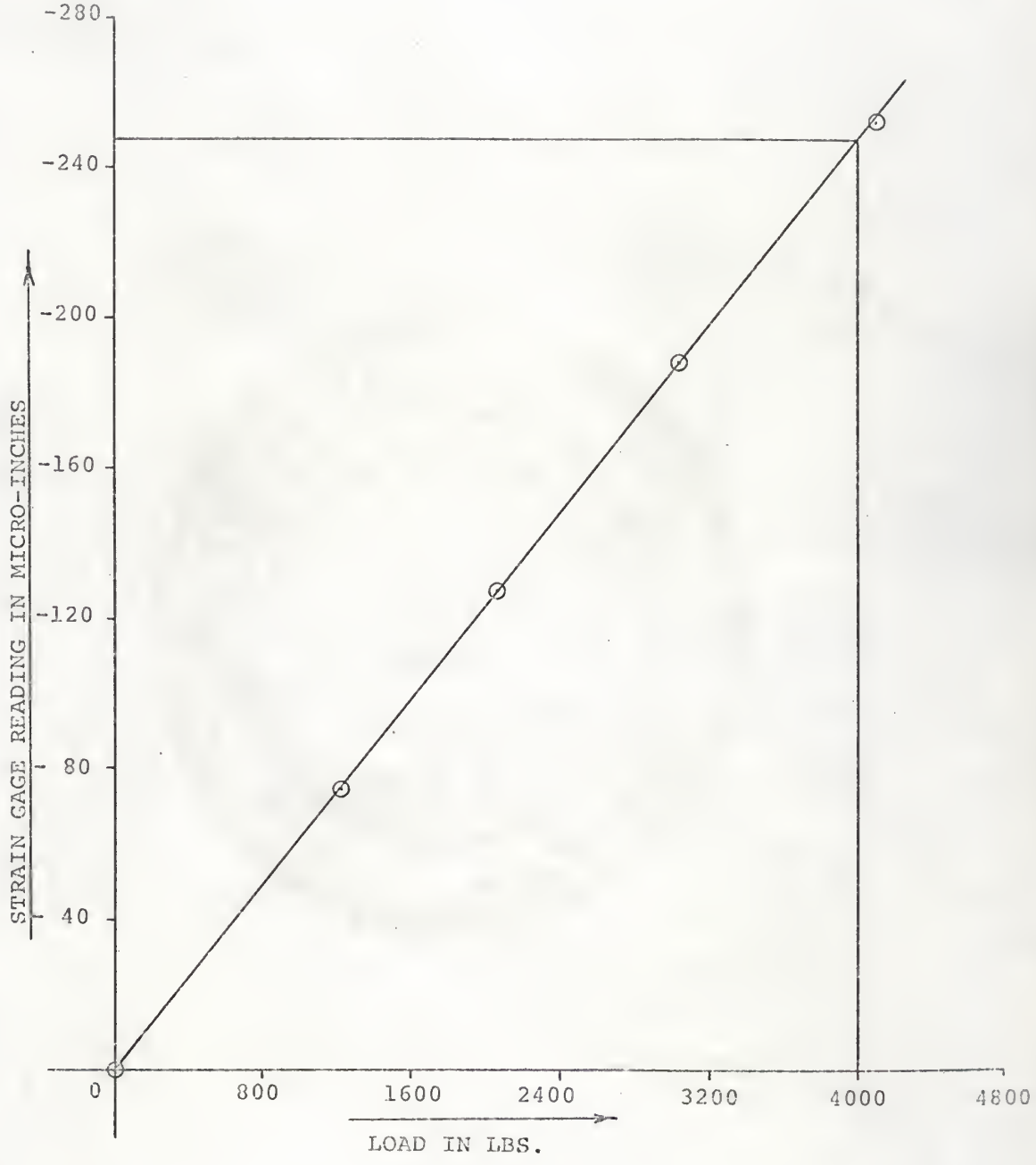

FIGURE 24. STRAIN GAGE READINGS FOR STRAIN GAGE NO. 8 AT FOUR LOAD LEVELS

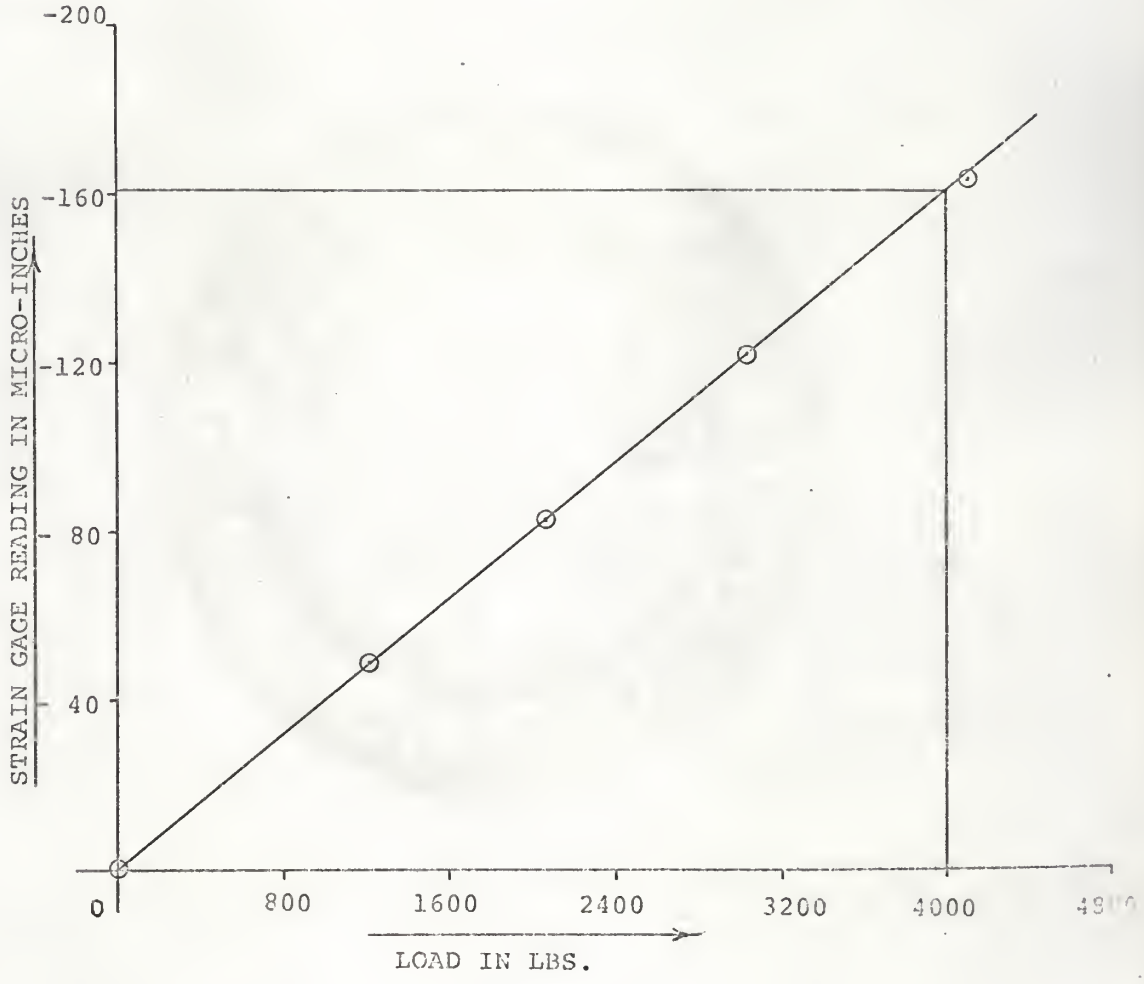

FIGURE 25. STRAIN GAGE READINGS FOR STRAIN GAGE NO. 9 AT FOUR LOAD LEVELS

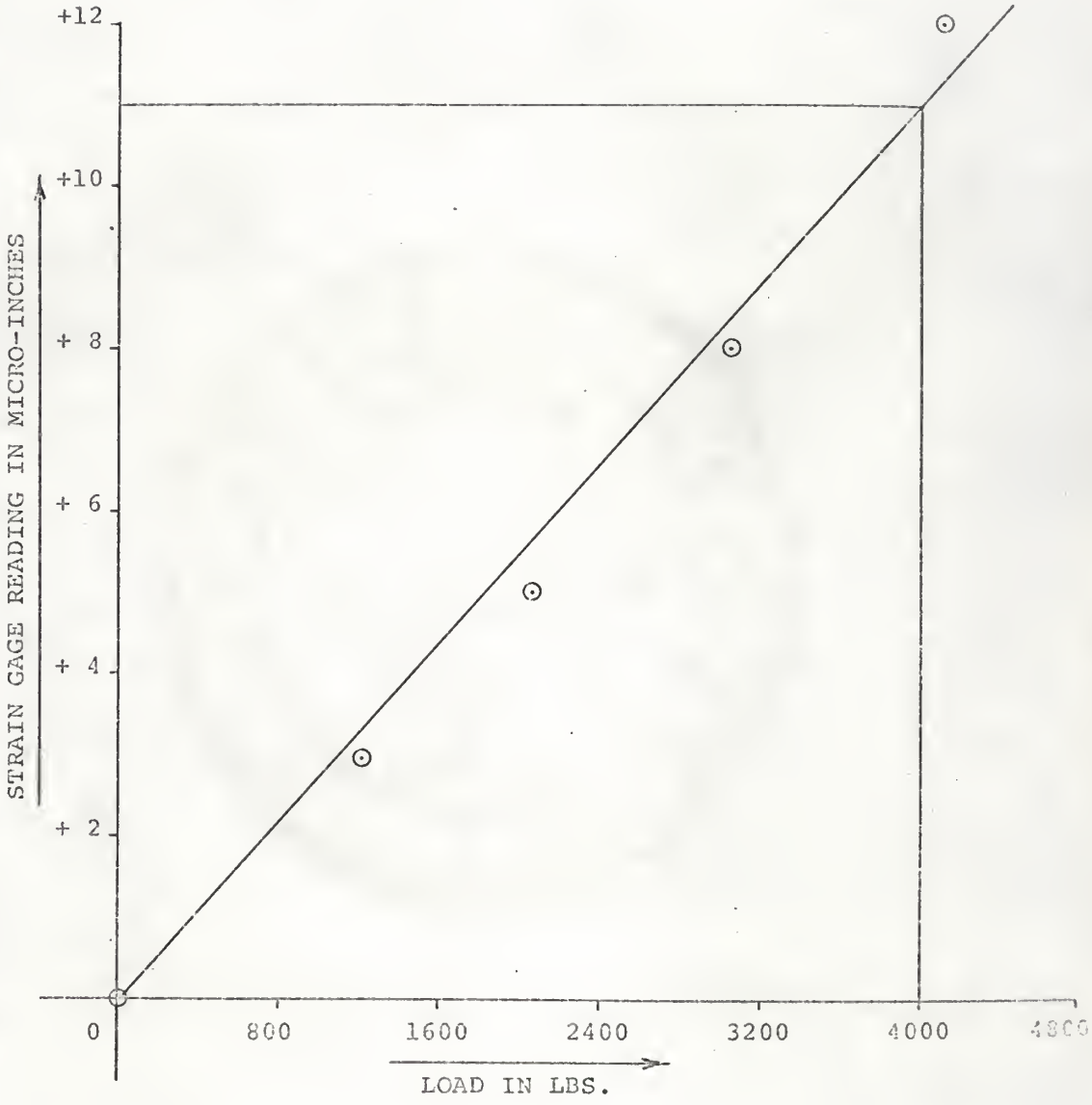

FIGURE 26. STRAIN GAGE READINGS FOR STRAIN GAGE NO. 0' AT FOUR LOAD LEVELS

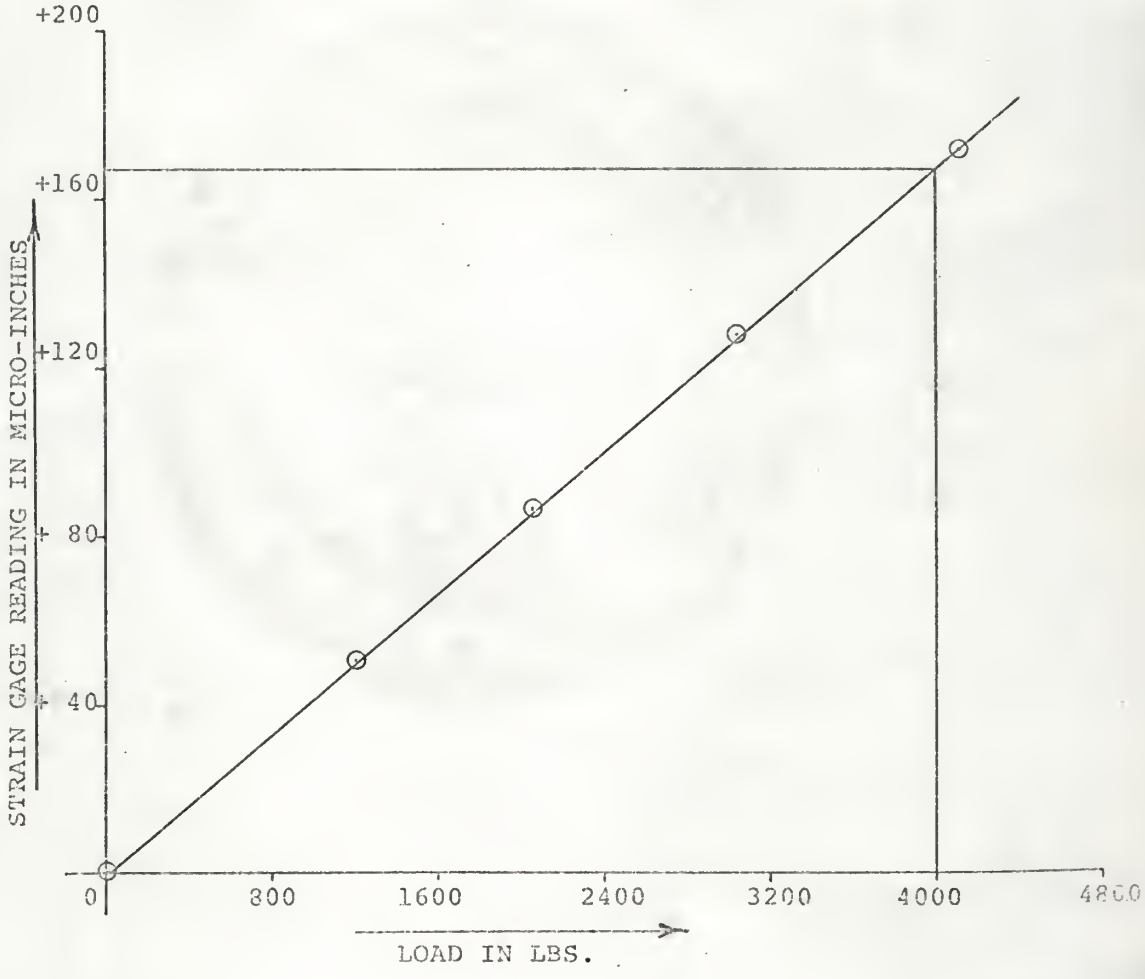

FIGURE 27. STRAIN GAGE READINGS FOR STRAIN GAGE NO. 1' AT FOUR LOAD LEVELS

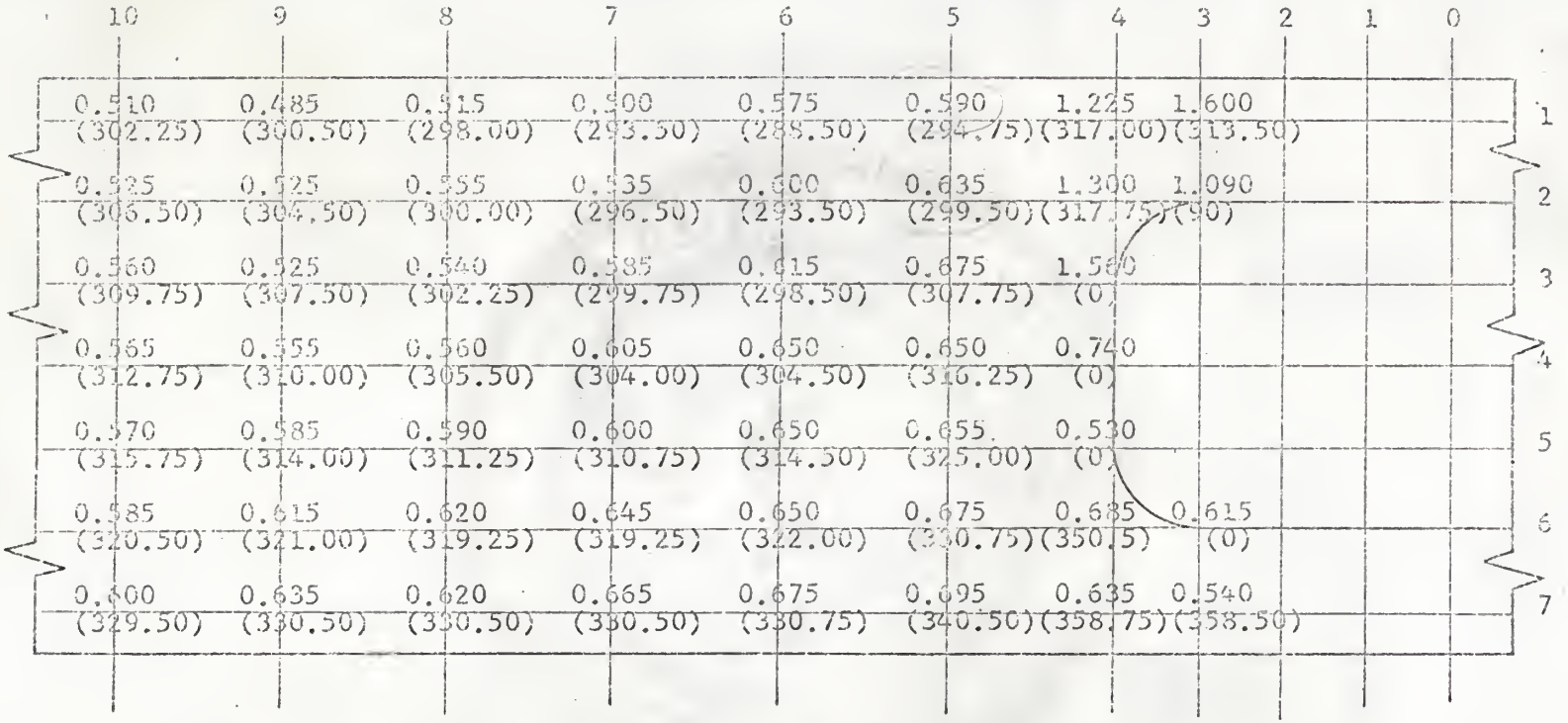

FIGURE 28. CORRECTED BIREFRINGENCE READINGS AND ISOCLINIC ANGLES (IN PARENTHESES) FOR 4000 LBS. LOAD

TABLE 3. INTERPOLATED STRAIN GAGE READINGS FOR 4000 LBS. LOAD WITH THE PLASTIC ON THE LEFT SIDE

STRAIN GAGE NO.	READING IN MICRO-INCHES
0	+415
1	+410
2	-365
3	-382
4	-368
5	-355
6	+410
7	+408
8	-248
9	-161
0'	+ 11
1'	+167

ANALYSIS OF DATA

Shear - Difference Method:

The shear-difference method was used to compute the normal stresses at the interior points of the web. This method is based on the equations of equilibrium for the two-dimensional stress state conditions. These equations are as follows:

$$\frac{\partial \sigma_x}{\partial x} + \frac{\partial S_{xy}}{\partial y} = 0, \qquad \frac{\partial \sigma_y}{\partial y} + \frac{\partial S_{xy}}{\partial x} = 0. \tag{6}$$

The solution of these equations can be written in the form

$$\sigma_x = (\sigma_x)_0 - \int \frac{\partial S_{xy}}{\partial y}\, dx, \qquad \sigma_y = (\sigma_y)_0 - \int \frac{\partial S_{xy}}{\partial x}\, dy. \tag{7}$$

$(\sigma_x)_0$ and $(\sigma_y)_0$ are the values of σ_x and σ_y at a given location for which the stresses are known or may be obtained. The values of the integrals in the above equations can be represented by the areas under the curves for which the ordinates are the rate of change of shear in the direction normal to the direction of integration and the abscissas are distances along the path of integration (Fig. 29a). In the case of a small finite particle, Fig. 29b, the integrals can be closely approximated by the following similar expressions containing summations of finite increments:

$$\sigma_x = (\sigma_x)_0 - \Sigma \frac{\Delta S_{xy}}{\Delta y}\, \Delta x, \qquad \sigma_y = (\sigma_y)_0 - \Sigma \frac{\Delta S_{xy}}{\Delta x}\, \Delta y. \tag{8}$$

These two equations provide the basic tools for the

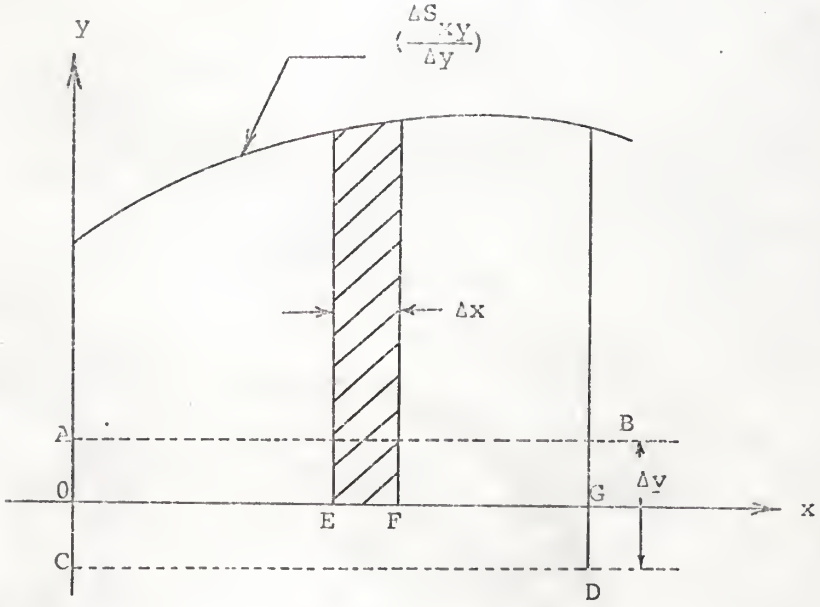

FIGURE 29a. SKETCH SHOWING DETERMINATION OF $(\Delta S_{xy})(\Delta x/\Delta y)$ BY THE SHEAR DIFFERENCE METHOD

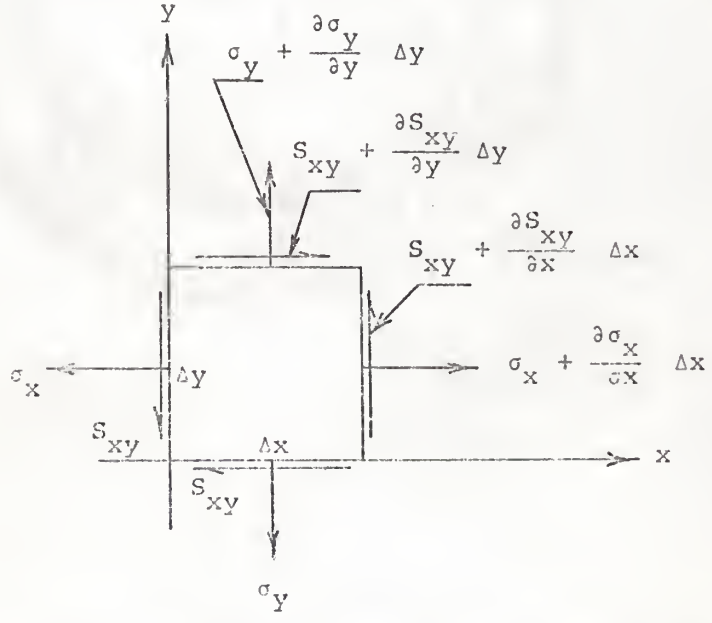

FIGURE 29b. STRESSES ACTING ON A SMALL RECTANGULAR ELEMENT IN THE X-Y PLANE

determination of the normal stresses, σ_x and σ_y, across arbitrary straight sections.

The system of co-ordinate axes chosen in the present case is shown in Fig. 30. Starting from the free boundary the normal stresses, σ_x and σ_y, were found at various points along horizontal section 4. Then starting from horizontal section 4, the stresses along various vertical sections were determined. The calculations for horizontal section 4 and vertical section 8 are shown here. The stresses along other vertical sections were found in a similar fashion.

The stresses along horizontal section 4 (Fig. 31) were found by starting from the free boundary (point 4,4). Assuming that the stresses had been computed up to point (4,6), the stress $(\sigma_x)_{4,7}$ was determined by the summation of horizontal forces as follows:

$$(\sigma_x)_{4,7} \cdot \Delta y + (S_{xy})_3 \cdot \Delta x - (\sigma_x)_{4,6} \cdot \Delta y - (S_{xy})_5 \Delta x = 0,$$

$$\text{or} \quad (\sigma_x)_{4,7} = (\sigma_x)_{4,6} - [(S_{xy})_3 - (S_{xy})_5] \frac{\Delta x}{\Delta y},$$

$$= (\sigma_x)_{4,6} - \Delta S_{xy} \cdot (\Delta x/\Delta y). \qquad (9)$$

Curves of shear stresses along horizontal section 3 and 5 were drawn on the same graph and the values of ΔS_{xy} for all the points along horizontal section 4 were measured from that graph. Then starting from the free boundary, where σ_x is zero, the value of σ_x for other points was calculated successively. The value of the transverse stress, σ_y, for any point can be computed from Mohr's circle of stresses (Fig. 32a) and is given by the following equation:

$$\sigma_y = \sigma_x \pm \sqrt{(\sigma_1 - \sigma_2)^2 - 4 S_{xy}^2}. \qquad (10)$$

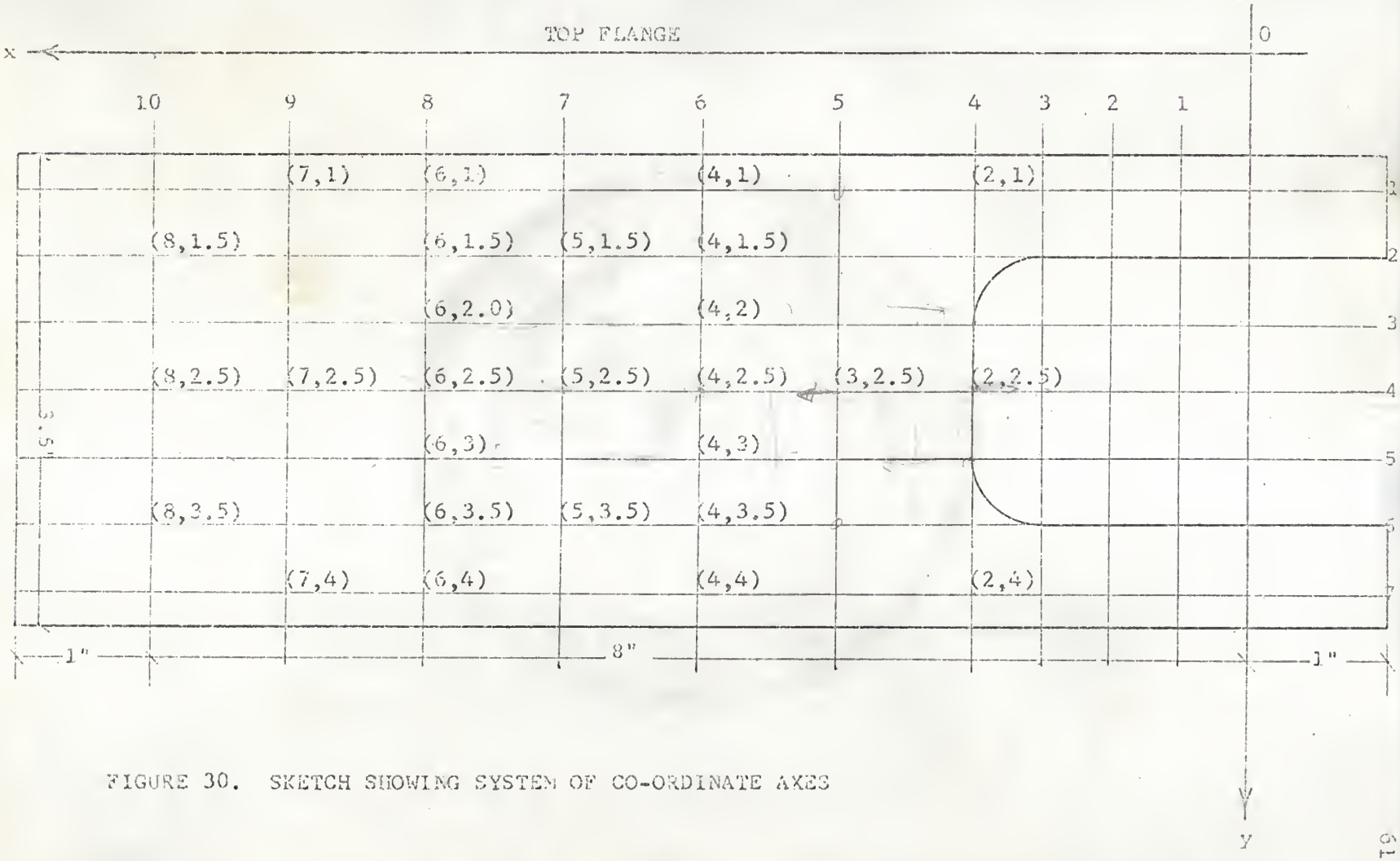

FIGURE 30. SKETCH SHOWING SYSTEM OF CO-ORDINATE AXES

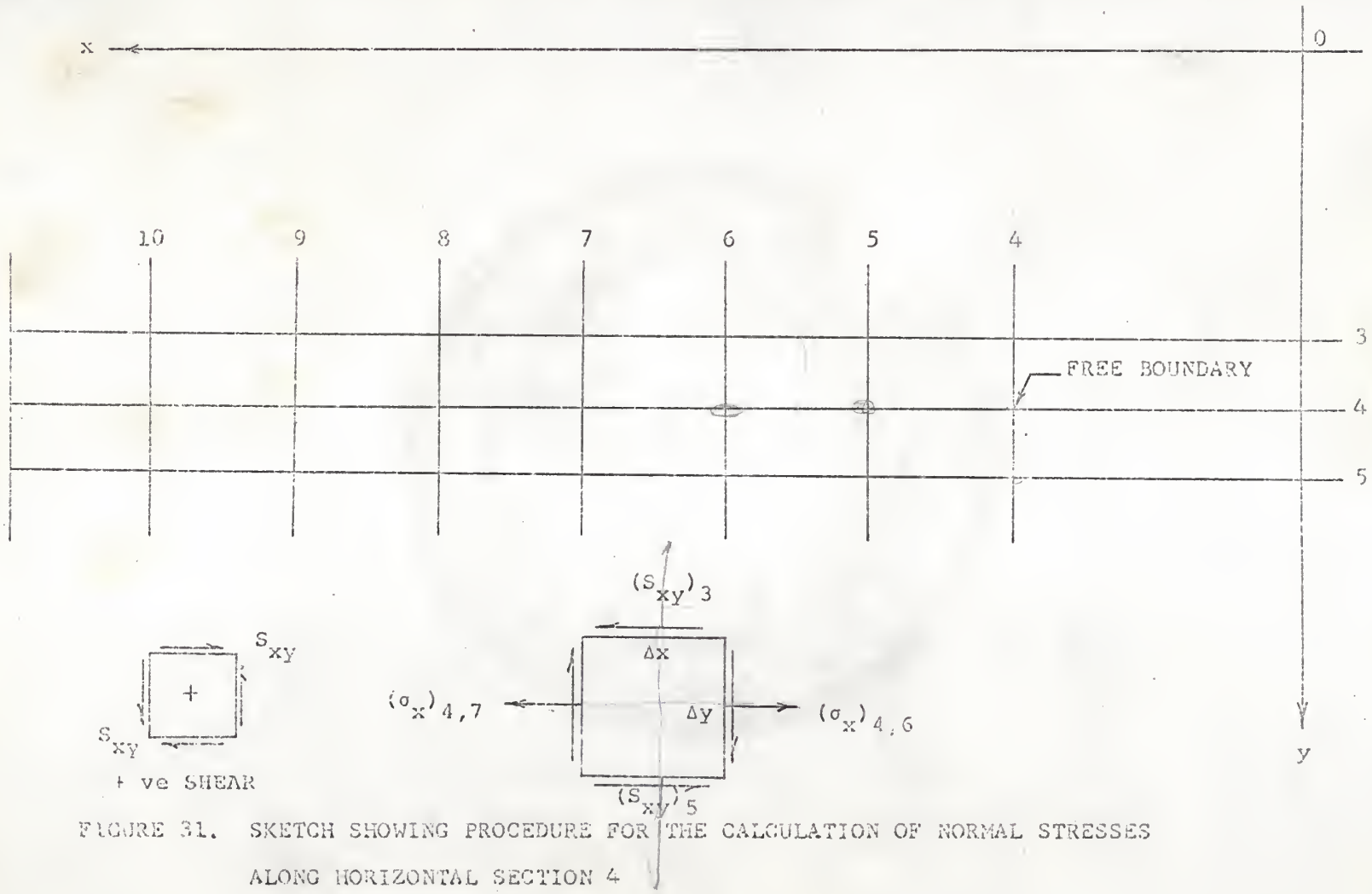

FIGURE 31. SKETCH SHOWING PROCEDURE FOR THE CALCULATION OF NORMAL STRESSES ALONG HORIZONTAL SECTION 4

The positive or negative sign in the above equation will be chosen depending upon the inclination of the major principal stress, σ_1 (Figs. 32b and 32c).

The normal stresses along any vertical section such as section 8 were found in a similar fashion by summing up forces in the vertical direction. Starting from any point along horizontal section 4 and going either up or down from there, the transverse stress, σ_y, was computed from the following equation:

$$\sigma_y = (\sigma_y)_4 - \Delta S_{xy}(\Delta y/\Delta x). \tag{11}$$

σ_x was then determined from the following relation:

$$\sigma_x = \sigma_y \pm \sqrt{(\sigma_1-\sigma_2)^2 - 4\, S_{xy}^2}\ . \tag{12}$$

Shear Stresses:

Referring to Mohr's circle of stresses (Fig. 32a), the shear stress in the X-Y plane at any point is given by

$$S_{xy} = (1/2)(\sigma_1-\sigma_2)\ \text{Sin}\ 2\ \theta \tag{13}$$

The photo-elastic method provides sufficient and necessary data to evaluate S_{xy} at any point. The principal stress difference, $(\sigma_1 - \sigma_2)$, is given by the isochromatic fringe pattern and the direction of principal stresses, θ, is given by the isoclinics. The direction of shear stress can be determined by examining the loading conditions and in the present case the sign of the shear stresses was negative throughout in the left half position. The values of the shear stresses were computed as shown in Table 4. The plots of these shear stresses for different sections are shown in Figs. 33 through 38 and for further calculations, the values

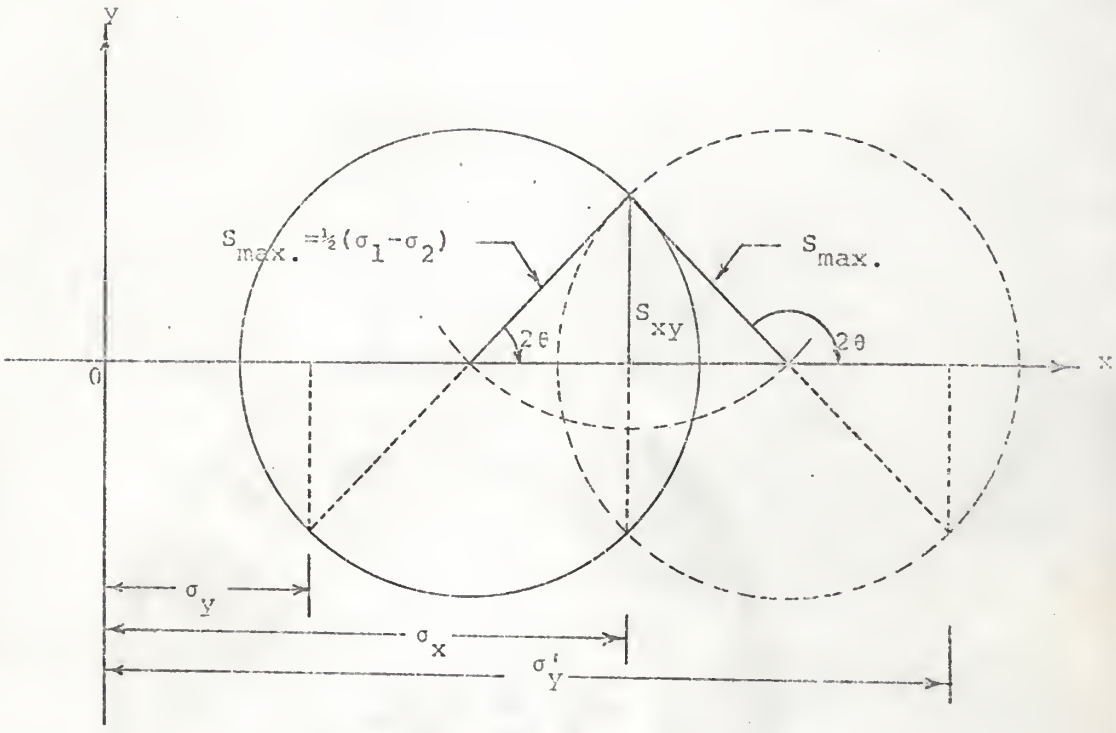

FIGURE 32a. SKETCH SHOWING TWO POSSIBLE CONSTRUCTIONS OF MOHR'S CIRCLE FOR THE SAME GIVEN $(\sigma_1-\sigma_2)$, σ_x AND S_{xy}

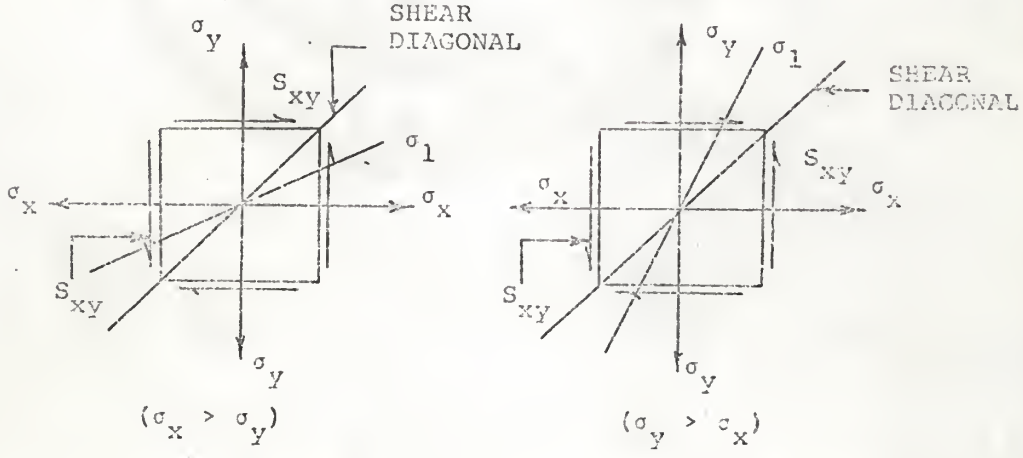

FIGURE 32b. SKETCH SHOWING RELATIVE MAGNITUDES OF σ_x AND σ_y

TABLE 4. CALCULATION OF SHEAR STRESSES

(1)	(2)	(3)	(4)	(5)	(6)	(7)
POINT	$(\sigma_1-\sigma_2)$ FRINGES	$(\sigma_1-\sigma_2)$ psi.	$\frac{1}{2}(\sigma_1-\sigma_2)$ psi.	θ DEGREES	Sin 2 θ	$S_{xy} = \frac{1}{2}(\sigma_1-\sigma_2)\times$ Sin 2 θ psi.
1,5	0.590	4970	2485	294.75	0.76041	-1890
2,5	0.635	5350	2675	299.50	0.85717	-2290
3,5	0.675	5680	2840	307.75	0.96815	-2755
4,5	0.650	5480	2740	316.25	0.99905	-2740
5,5	0.655	5520	2760	325.00	0.93969	-2590
6,5	0.675	5680	2840	330.75	0.85264	-2425
7,5	0.695	5850	2925	340.50	0.62932	-1835
1,6	0.575	4840	2420	288.50	0.60181	-1460
2,6	0.600	5050	2525	293.50	0.73135	-1850
3,6	0.615	5180	2590	298.50	0.83867	-2170
4,6	0.650	5480	2740	304.50	0.93358	-2560
5,6	0.650	5480	2740	314.50	0.99985	-2740
6,6	0.650	5480	2740	322.00	0.97029	-2560
7,6	0.675	5680	2840	330.75	0.85264	-2425
1,7	0.500	4210	2105	293.50	0.73135	-1540
2,7	0.535	4510	2255	296.50	0.79863	-1810
3,7	0.585	4930	2465	299.75	0.86163	-2050
4,7	0.605	5090	2550	304.00	0.92718	-2365
5,7	0.600	5050	2525	310.75	0.98769	-2490
6,7	0.645	5430	2715	319.25	0.98769	-2680
7,7	0.665	5590	2795	330.50	0.85717	-2405

TABLE 4. CALCULATION OF SHEAR STRESSES CONTINUED

(1)	(2)	(3)	(4)	(5)	(6)	(7)
POINT	$(\sigma_1-\sigma_2)$ FRINGES	$(\sigma_1-\sigma_2)$ psi.	$\frac{1}{2}(\sigma_1-\sigma_2)$ psi.	θ DEGREES	Sin 2.θ	$S_{xy} = \frac{1}{2}(\sigma_1-\sigma_2)x$ Sin 2θ psi.
1,8	0.515	4340	2170	298.00	0.82904	-1800
2,8	0.555	4670	2335	300.00	0.86603	-2060
3,8	0.540	4550	2275	302.25	0.90258	-2055
4,8	0.560	4720	2360	305.50	0.94552	-2226
5,8	0.590	4960	2480	311.25	0.99144	-2460
6,8	0.620	5220	2610	319.25	0.98901	-2560
7,8	0.620	5220	2610	330.50	0.85717	-2240
1,9	0.485	4080	2040	300.50	0.87462	-1785
2,9	0.525	4420	2210	304.50	0.93358	-2060
3,9	0.525	4420	2210	307.50	0.96592	-2135
4,9	0.555	4670	2335	310.00	0.98481	-2300
5,9	0.585	4930	2465	314.00	0.99939	-2460
6,9	0.615	5180	2590	321.00	0.97815	-2530
7,9	0.635	5350	2675	330.50	0.87462	-2300
1,10	0.510	4300	2150	302.25	0.90258	-1940
2,10	0.525	4420	2210	306.50	0.95630	-2110
3,10	0.560	4720	2360	309.75	0.98325	-2320
4,10	0.565	4760	2380	312.75	0.99692	-2370
5,10	0.570	4800	2400	315.75	0.99966	-2400
6,10	0.585	4930	2465	320.50	0.98163	-2420
7,10	0.600	5050	2525	329.50	0.87462	-2210

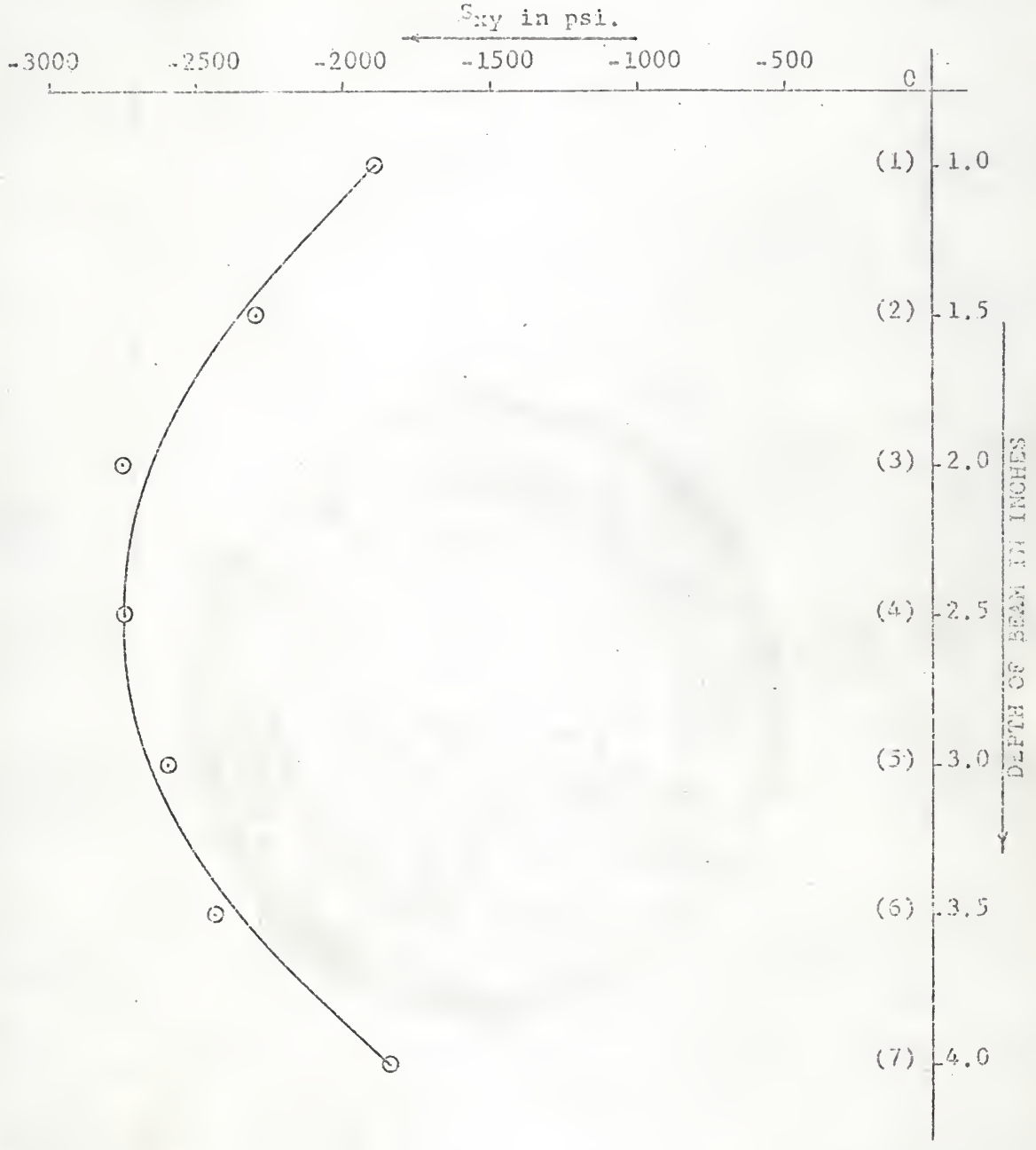

FIGURE 33. SHEAR STRESS DISTRIBUTION FOR VERTICAL SECTION 5
(NUMBERS IN PARENTHESES SHOW HORIZONTAL SECTION)

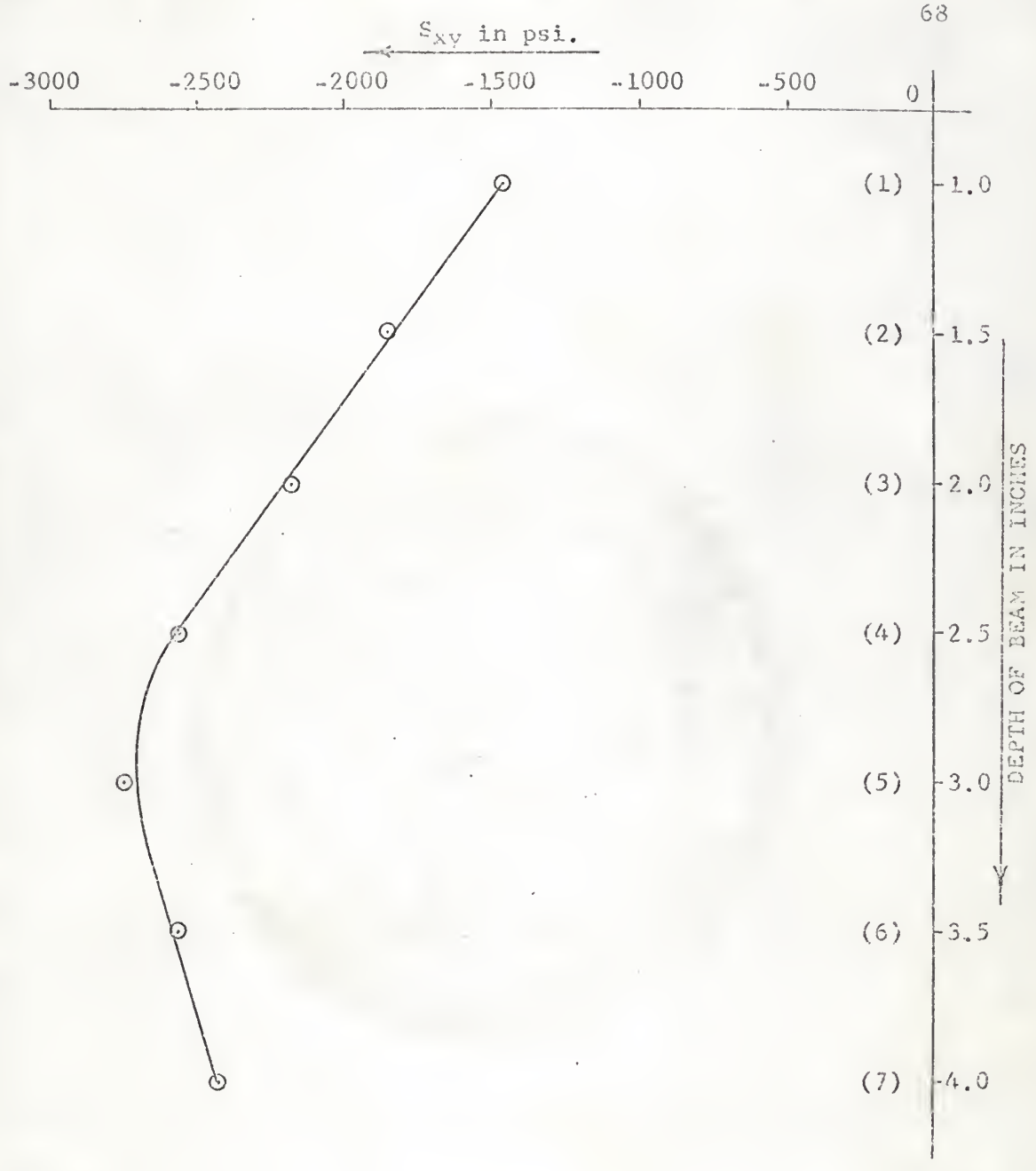

FIGURE 34. SHEAR STRESS DISTRIBUTION FOR VERTICAL SECTION 6
(NUMBERS IN PARENTHESES SHOW HORIZONTAL SECTION)

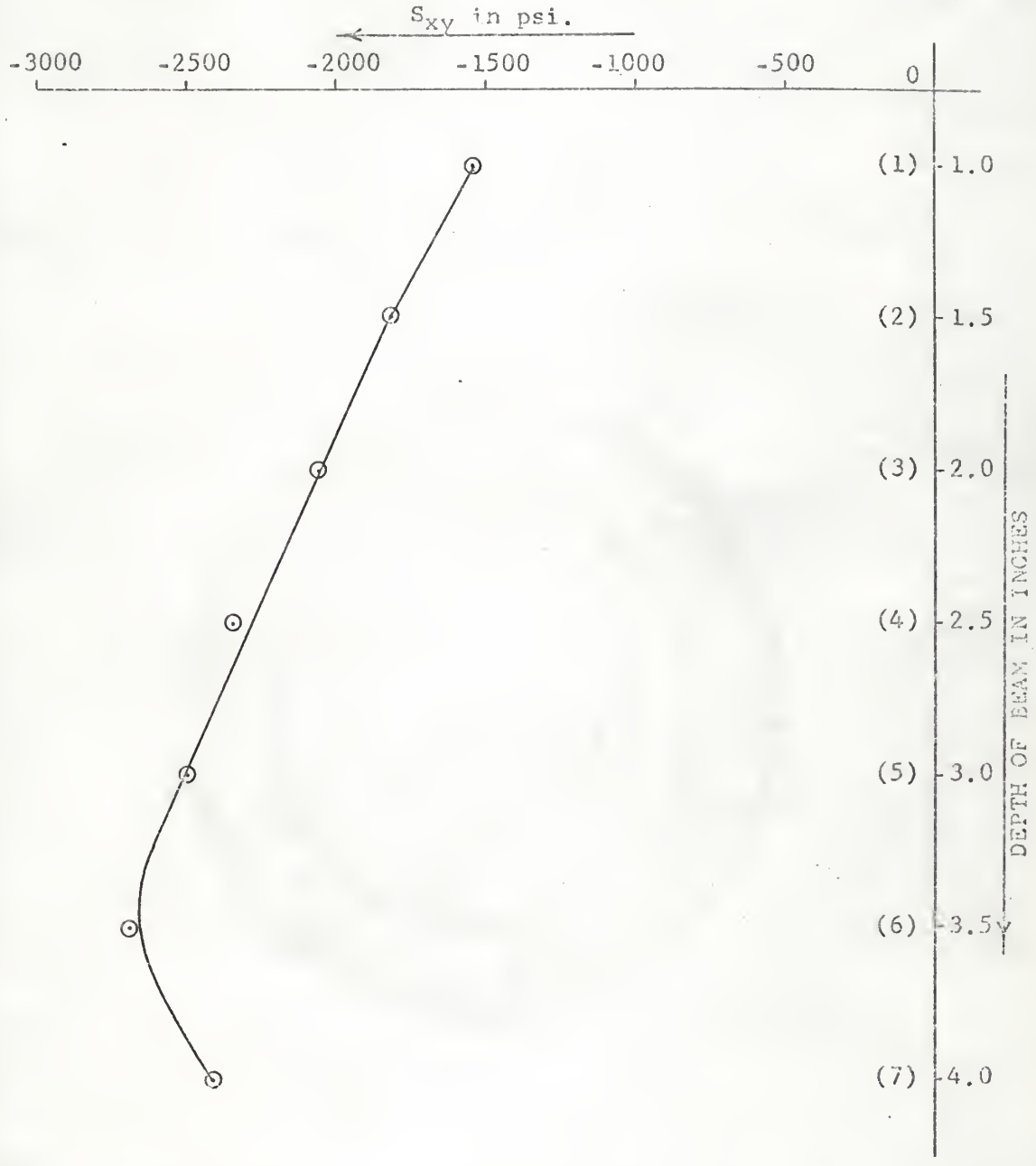

FIGURE 35. SHEAR STRESS DISTRIBUTION FOR VERTICAL SECTION 7
(NUMBERS IN PARENTHESES SHOW HORIZONTAL SECTION)

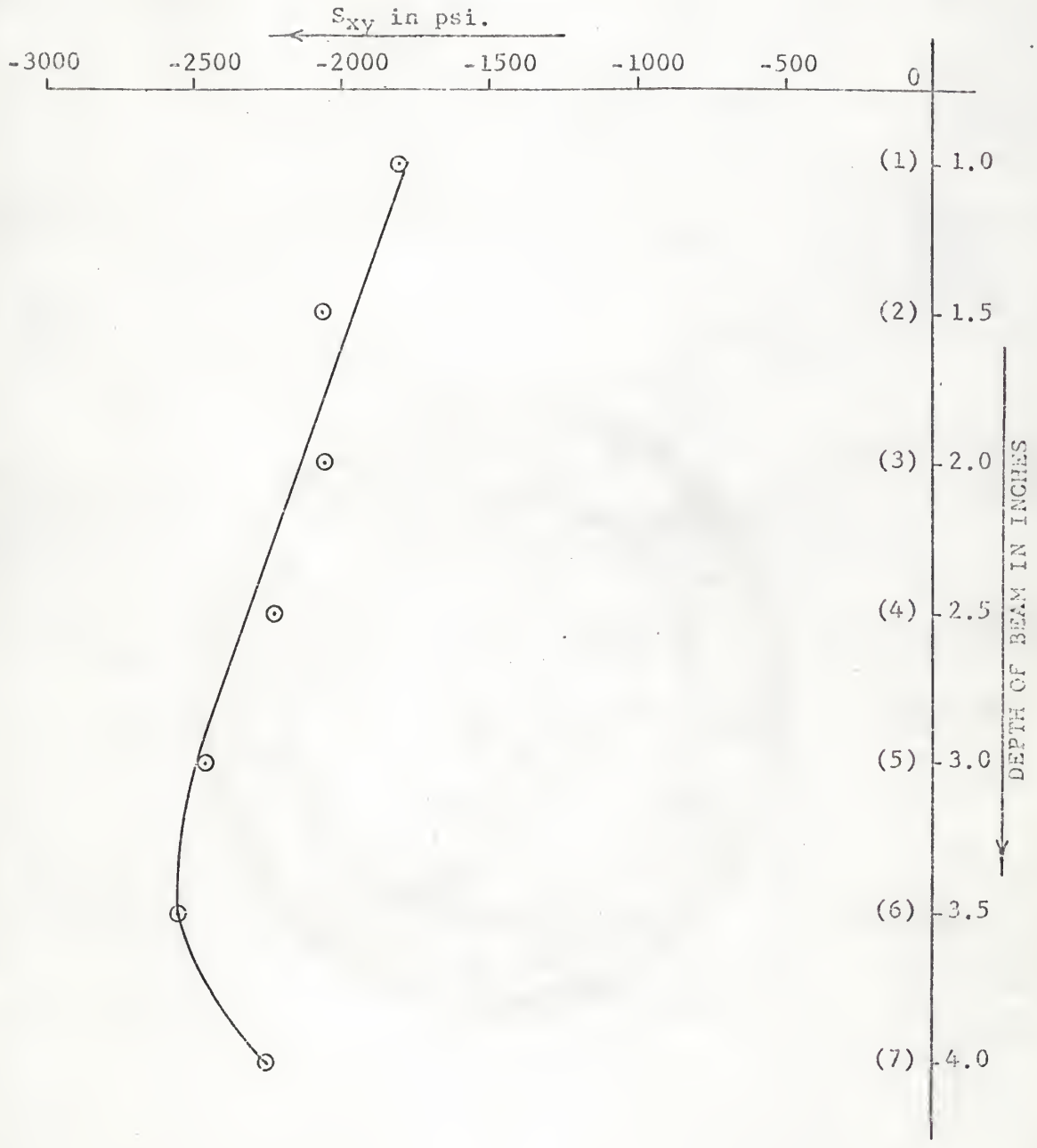

FIGURE 36. SHEAR STRESS DISTRIBUTION FOR VERTICAL SECTION 8
(NUMBERS IN PARENTHESES SHOW HORIZONTAL SECTION)

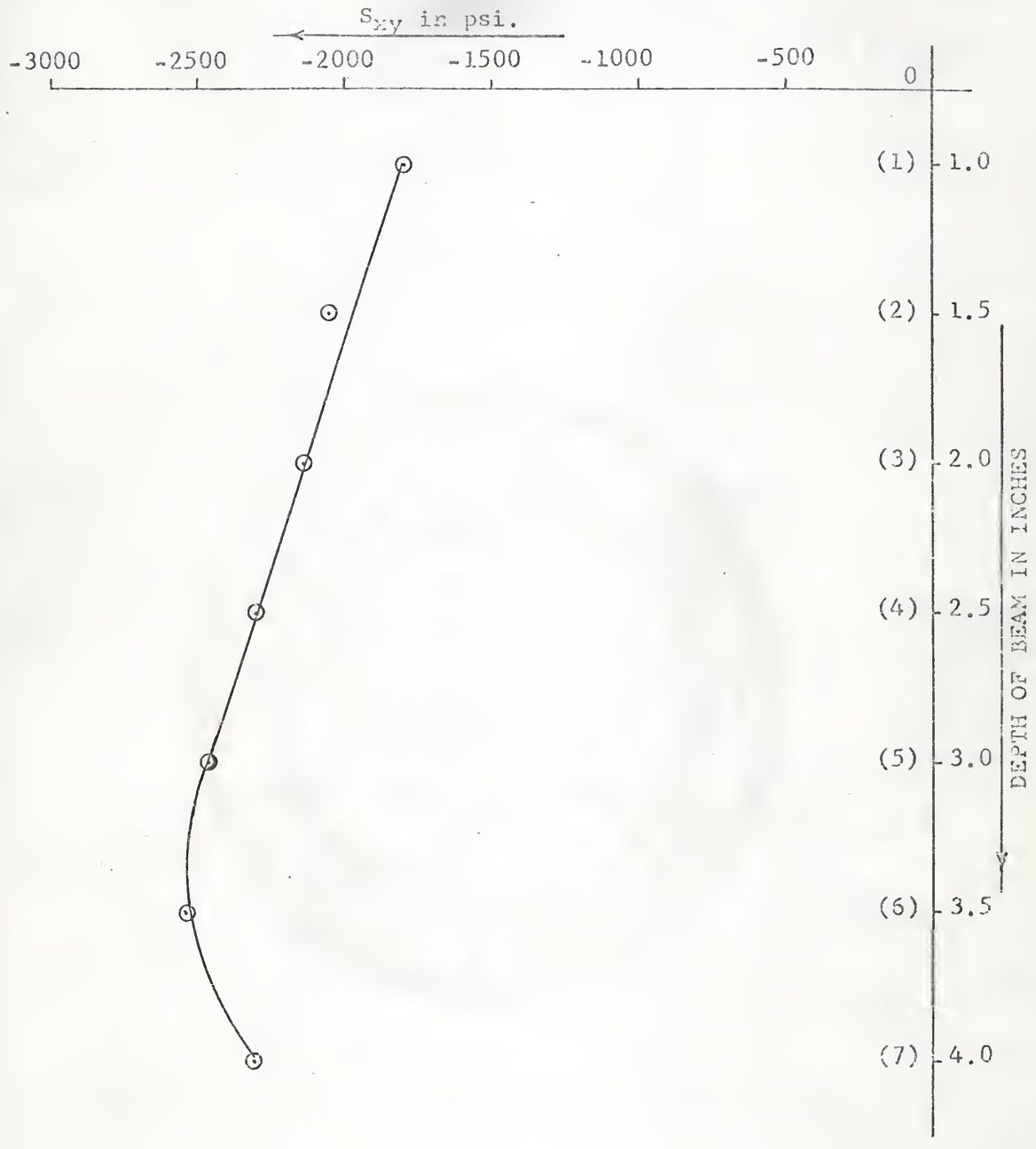

FIGURE 37. SHEAR STRESS DISTRIBUTION FOR VERTICAL SECTION 9
(NUMBERS IN PARENTHESES SHOW HORIZONTAL SECTION)

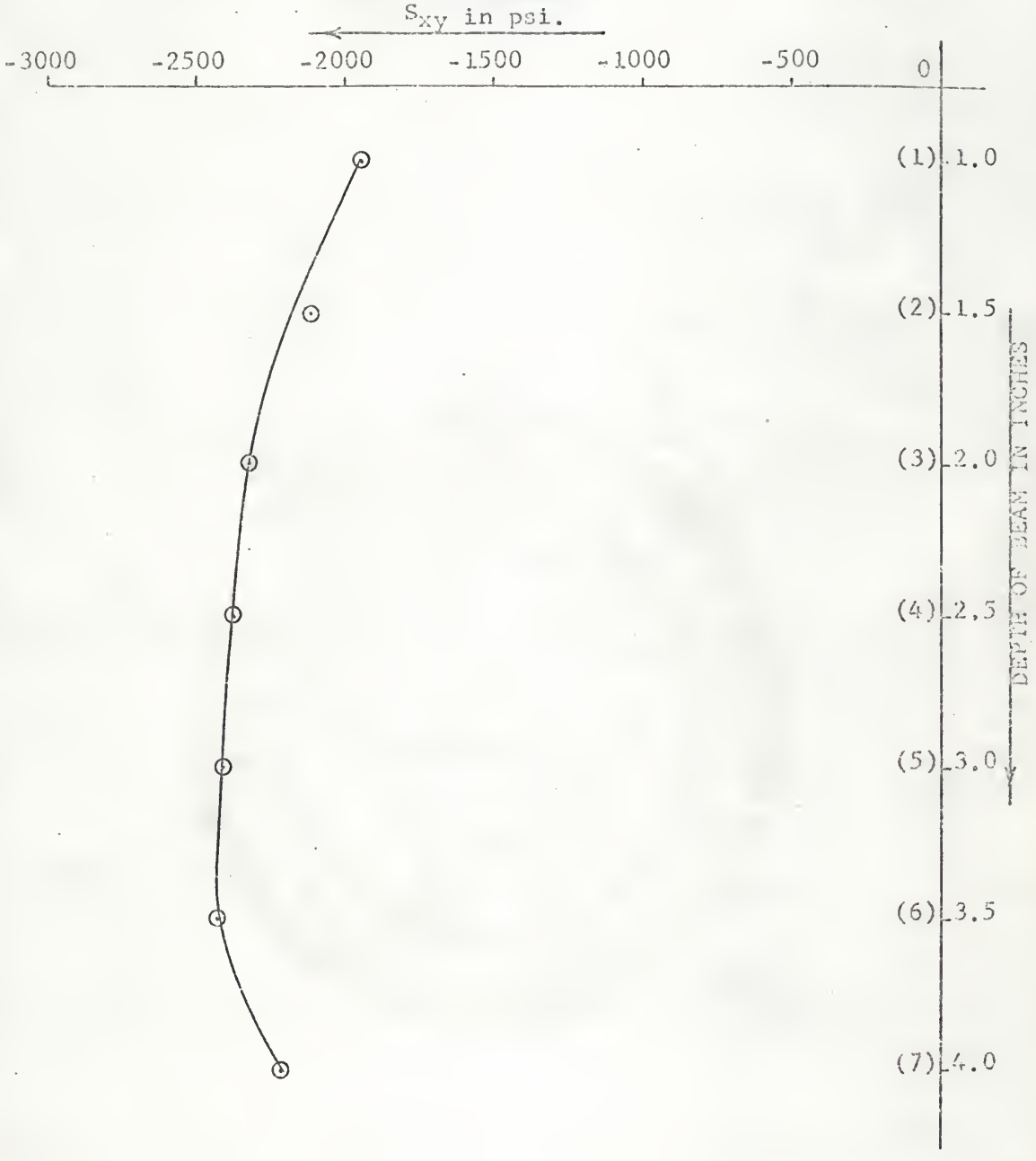

FIGURE 38. SHEAR STRESS DISTRIBUTION FOR VERTICAL SECTION 10
(NUMBERS IN PARENTHESES SHOW HORIZONTAL SECTION)

of shear stresses from these curves were used.

Stresses Along Horizontal Section 4:

In order to compute the stresses along horizontal section 4, curves for shear stresses along horizontal sections 3 and 5 were drawn (Fig. 39). The values of ΔS_{xy} for each point were then measured from that figure. In going from horizontal section 3 to horizontal section 5, the sign of ΔS_{xy} for point 4,5 was negative and for point 4,6 and beyond it was positive. These values were as follows:

$$(\Delta S_{xy})_{4,5} = -1700 - (-1430) = -270 \text{ psi},$$

$$(\Delta S_{xy})_{4,6} = -2410 - (-2710) = +300 \text{ psi},$$

$$(\Delta S_{xy})_{4,7} = -2145 - (-2595) = +450 \text{ psi},$$

$$(\Delta S_{xy})_{4,8} = -2075 - (-2485) = +410 \text{ psi},$$

$$(\Delta S_{xy})_{4,9} = -2120 - (-2430) = +310 \text{ psi},$$

$$(\Delta S_{xy})_{4,10} = -2240 - (-2410) = +170 \text{ psi}.$$

The value of Δx in going from left to right was positive for all points according to the system of co-ordinates chosen, Fig. 30. The values of Δy were also positive in going from horizontal section 3 to 5. The values of Δx and Δy were

$$(\Delta x)^3_{4,5} = 3 - 2 = +1.$$

$$(\Delta y)^3_{4,5} = 3 - 2 = +1.$$

The values of Δx and Δy were the same for all other points because of the uniformity of the grid pattern. The calculations for normal stresses along horizontal section 4 are shown in Table 5.

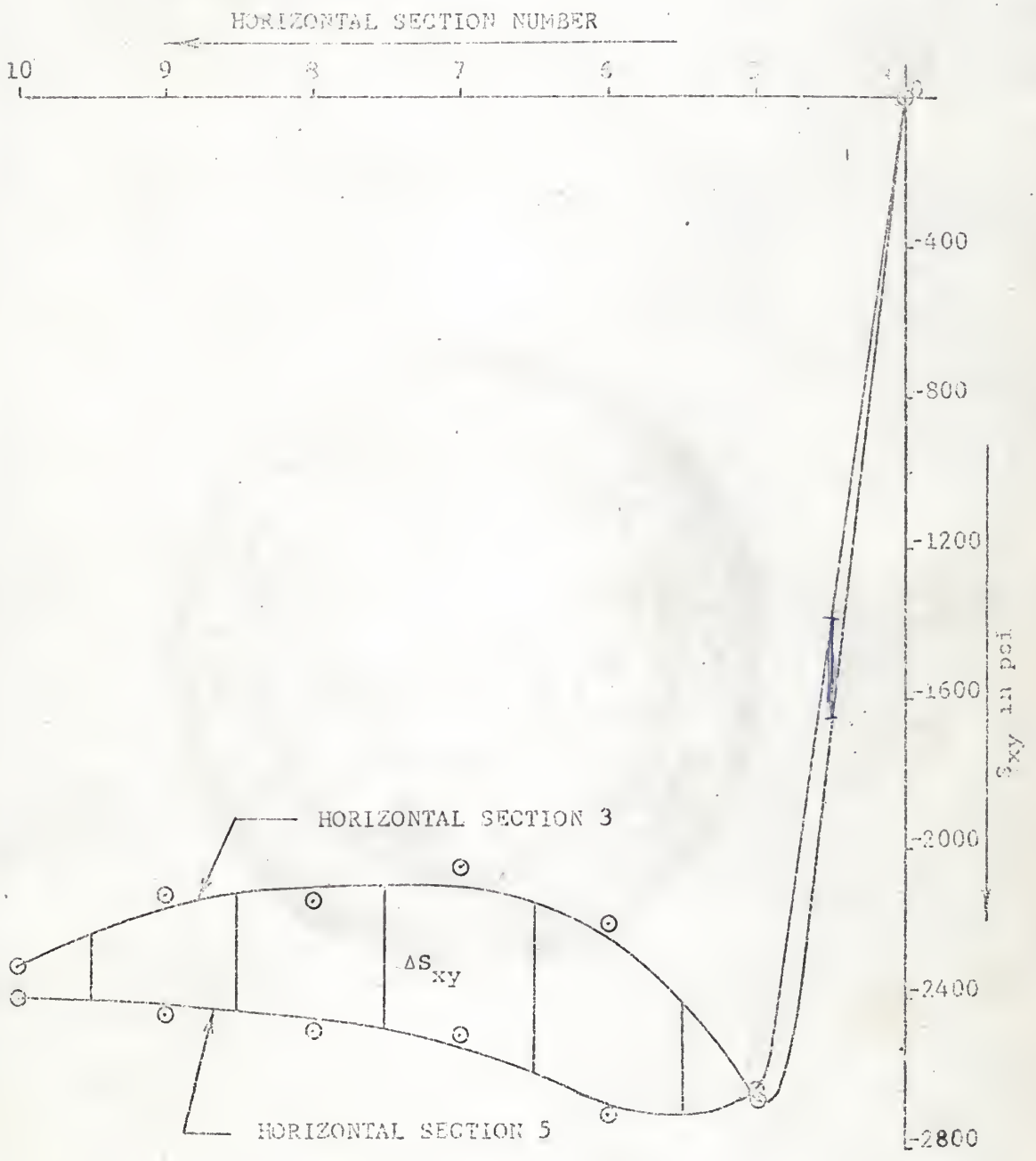

FIGURE 39. VALUES OF ΔS_{xy} FOR CALCULATION OF NORMAL STRESSES ALONG HORIZONTAL SECTION 4

TABLE 5. CALCULATION OF NORMAL STRESSES ALONG HORIZONTAL SECTION 4

(1)	(2)	(3)	(4)	(5)	(6)	(7)	(8)	(9)
POINT	$\Delta S_{xy}/\Delta x$	σ_x psi.	$(\sigma_1-\sigma_2)$ psi.	S_{xy} psi.	$(\sigma_1-\sigma_2)^2$ (x 10^2)	$4\,S_{xy}^2$ (x 10^2)	$\sqrt{(\sigma_1-\sigma_2)^2-4\,S_{xy}^2}$ psi.	$\sigma_y=\sigma_x \pm \sqrt{(\sigma_1-\sigma_2)^2-4\,S_{xy}^2}$ psi.
4,4	--	0	5240	0	389376	0	6240	-6240
4,5	-270	+270	5480	2740	300304	300304	0	+ 270
4,6	+300	- 30	5480	2575	300304	265225	1870	+1840
4,7	+450	-480	5090	2280	259081	207936	2260	+1780
4,8	+410	-890	4720	2320	222784	215296	865	- 25
4,9	+310	-1200	4670	2290	218089	209764	910	- 290
4,10	+170	-1370	4760	2370	226576	224676	445	- 615

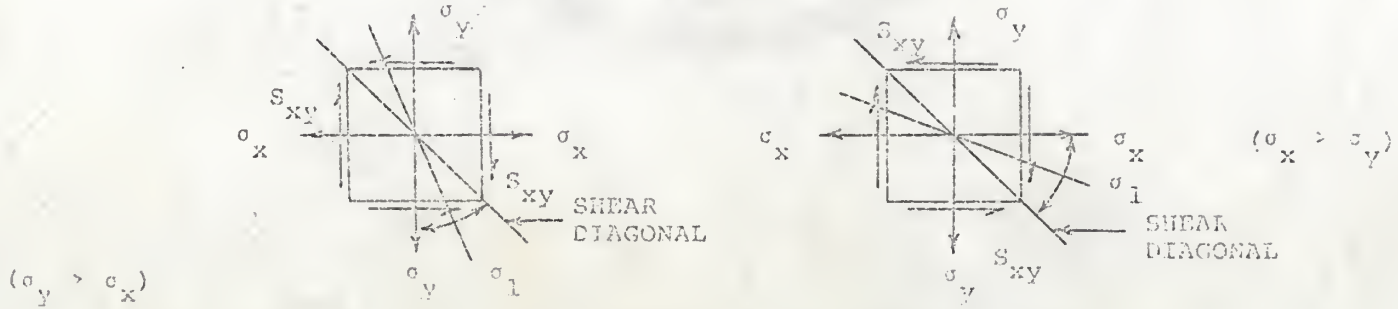

SKETCH SHOWING RELATIVE MAGNITUDES OF σ_x AND σ_y

Stresses Along Vertical Section 8:

Knowing the stresses at point (4,8), the stresses at other points along the vertical section 8 were computed. For that purpose curves of shear stresses along vertical sections 7 and 9 were drawn (Fig. 40) on the same graph and the various values of ΔS_{xy} were measured from there. The values of ΔS_{xy} while working upwards from point (4,8) and going from vertical section 9 to vertical section 7 were as follows:

$$(\Delta S_{xy})_{3,8} = -2215 - (-2155) = -60 \text{ psi},$$

$$(\Delta S_{xy})_{2,8} = -2055 - (-1935) = -120 \text{ psi},$$

$$(\Delta S_{xy})_{1,8} = -1875 - (-1680) = -195 \text{ psi}.$$

The similar values while working downwards from point (4,8) were:

$$(\Delta S_{xy})_{5,8} = -2370 - (-2370) = 0 \text{ psi},$$

$$(\Delta S_{xy})_{6,8} = -2500 - (-2600) = +100 \text{ psi},$$

$$(\Delta S_{xy})_{7,8} = -2420 - (-2580) = +160 \text{ psi}.$$

The values of the normal stresses were computed from Eqs. 11 and 12. Table 6 shows the calculations for stresses at various points along the vertical section 8. It also shows the values and signs of Δx and Δy. The normal stresses along other vertical sections were found by a similar procedure; i.e., by starting from the corresponding point on horizontal section 4.

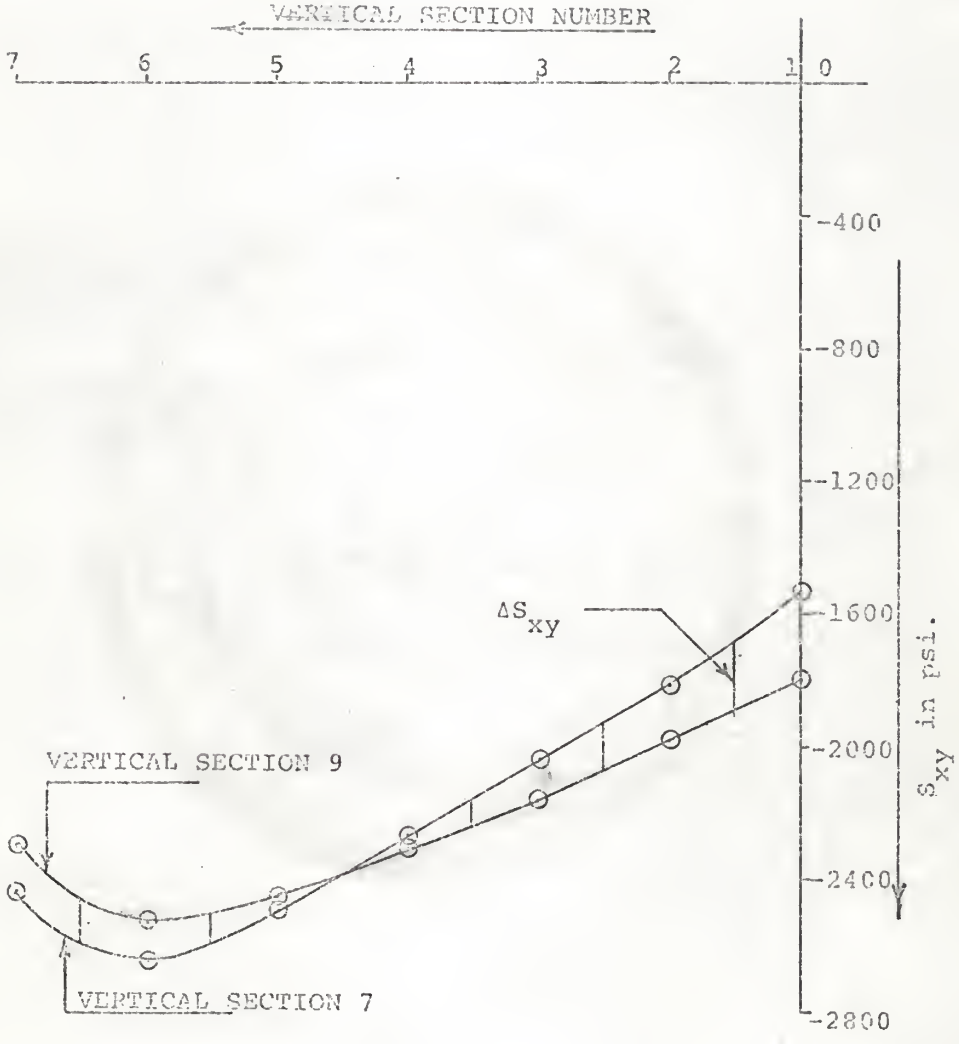

FIGURE 40. VALUES OF ΔS_{xy} FOR CALCULATION OF NORMAL STRESSES ALONG VERTICAL SECTION 8

TABLE 6. CALCULATION OF NORMAL STRESSES ALONG VERTICAL SECTION 8

(1)	(2)	(3)	(4)	(5)	(6)	(7)	(8)	(9)	(10)	(11)	(12)	(13)
PT.	Δx inch	Δy in.	$\frac{\Delta y}{\Delta x}$	ΔS_{xy} psi	$\Delta S_{xy}\frac{\Delta y}{\Delta x}$ psi	σ_y psi	$(\sigma_1-\sigma_2)$ psi	S_{xy} psi	$(\sigma_1-\sigma_2)^2$ $(\times 10^2)$	$4\,S_{xy}^2$ $(\times 10^2)$	$\sqrt{(10)-(11)}$	$\sigma_x = (7)\pm(12)$ psi
4,8	--	--	--	--	--	-25	4720	2320	222784	215296	865	- 890
3,8	-2	-½	+¼	- 60	-15	-10	4550	2140	207025	183184	1540	-1550
2,8	-2	-½	+¼	-120	-30	+20	4670	1950	218089	152100	2570	-2550
1,8	-2	-½	+¼	-195	-49	+69	4340	1775	188356	126025	2500	-2431
4,8	--	--	--	--	--	-25	4720	2320	222784	215296	865	- 890
5,8	-2	+½	-¼	0	0	-25	4960	2480	246016	246016	0	- 25
6,8	-2	+½	-¼	+100	-25	+ 0	5220	2540	272484	258064	1200	+1200
7,8	-2	+½	-¼	+160	-40	+40	5220	2250	272484	202500	2645	+2685

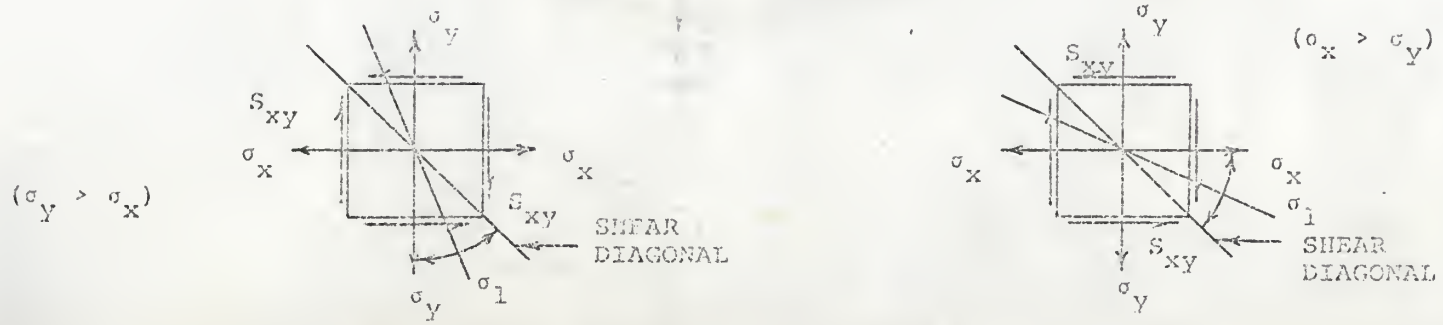

SKETCH SHOWING RELATIVE MAGNITUDES OF σ_x AND σ_y

PRESENTATION OF RESULTS

Figures 42 through 46 show the distribution of stresses across various sections of the beam. In these figures, curve I shows the distribution of longitudinal stress, σ_x, calculated photo-elastically, curve II shows the distribution of longitudinal stress, σ_x, calculated on the basis of common flexure theory, curve III shows the distribution of transverse stress, σ_y, calculated photo-elastically, curve IV shows the distribution of shear stress, S_{xy}, calculated on the basis of simple beam theory and curve V shows the distribution of shear stress calculated from photo-elastic data. The values of shear and longitudinal stresses according to simple beam theory can be calculated from Fig. 41. Since, according to simple beam theory, shear force remains constant from the reaction to the load, the values of the shear stresses for each vertical section will remain the same and can be calculated from the following relationship:

$$S_{xy} = (VQ)/(Ib). \qquad (14)$$

Longitudinal stress for the various sections can be calculated from the relationship:

$$\sigma_x = (M/I)y. \qquad (15)$$

V is the shear force at the section.

Q is the static moment of the remaining area above or below the neutral axis.

I is the amount of inertia about the axis of bending.

b is the width of the section.

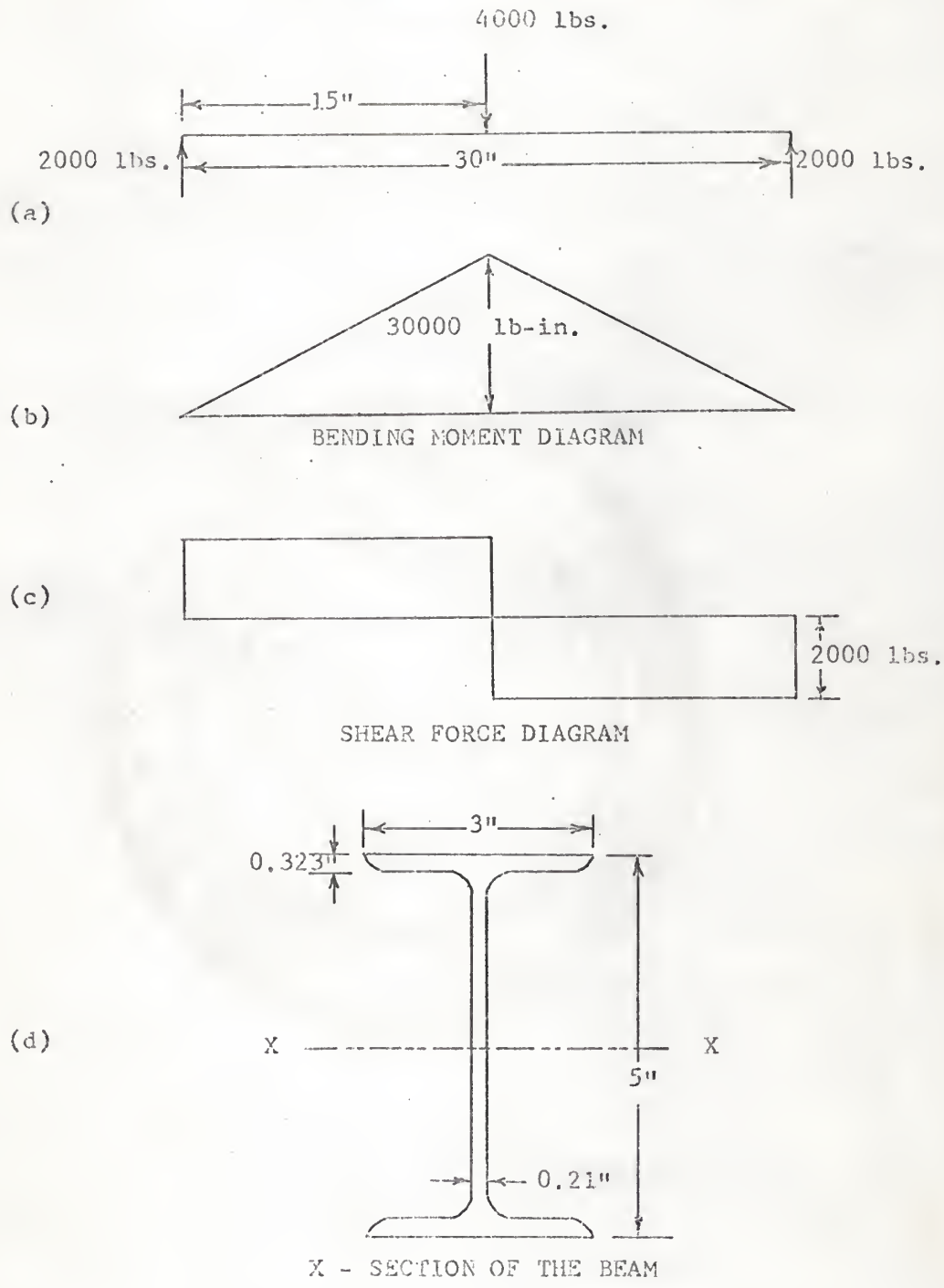

FIGURE 41. SKETCH SHOWING BENDING MOMENT AND SHEAR FORCE DIAGRAMS AND X-SECTION OF THE BEAM

M is the moment at the section.

y is the fiber distance from the neutral axis.

The distribution of stresses for section 8 are shown in Fig. 45. This figure has an extra curve VI. This curve was obtained from the strain gage calculations. Table 7 shows the calculation of stresses, for 4000 lbs. load, from the strain gages. The average value of the strain gage readings for the compression and tension flanges were taken from Table 3.

TABLE 7. CALCULATION OF STRESSES FROM STRAIN GAGE READINGS

STRAIN GAGE AT	CO-ORDINATES INCHES	STRAIN GAGE READING MICRO-INCHES	LONGITUDINAL STRESS σ_x psi
UPPER FLANGE	($\pm$ 6, 0)	-368	-3680
8	(6, 1.25)	-248	-2480
9	(6, 2)	-161	-1610
0'	(6, 3)	+ 11	+ 110
1'	(6, 3.75)	+167	+1670
LOWER FLANGE	($\pm$ 6, 5)	+411	+4110

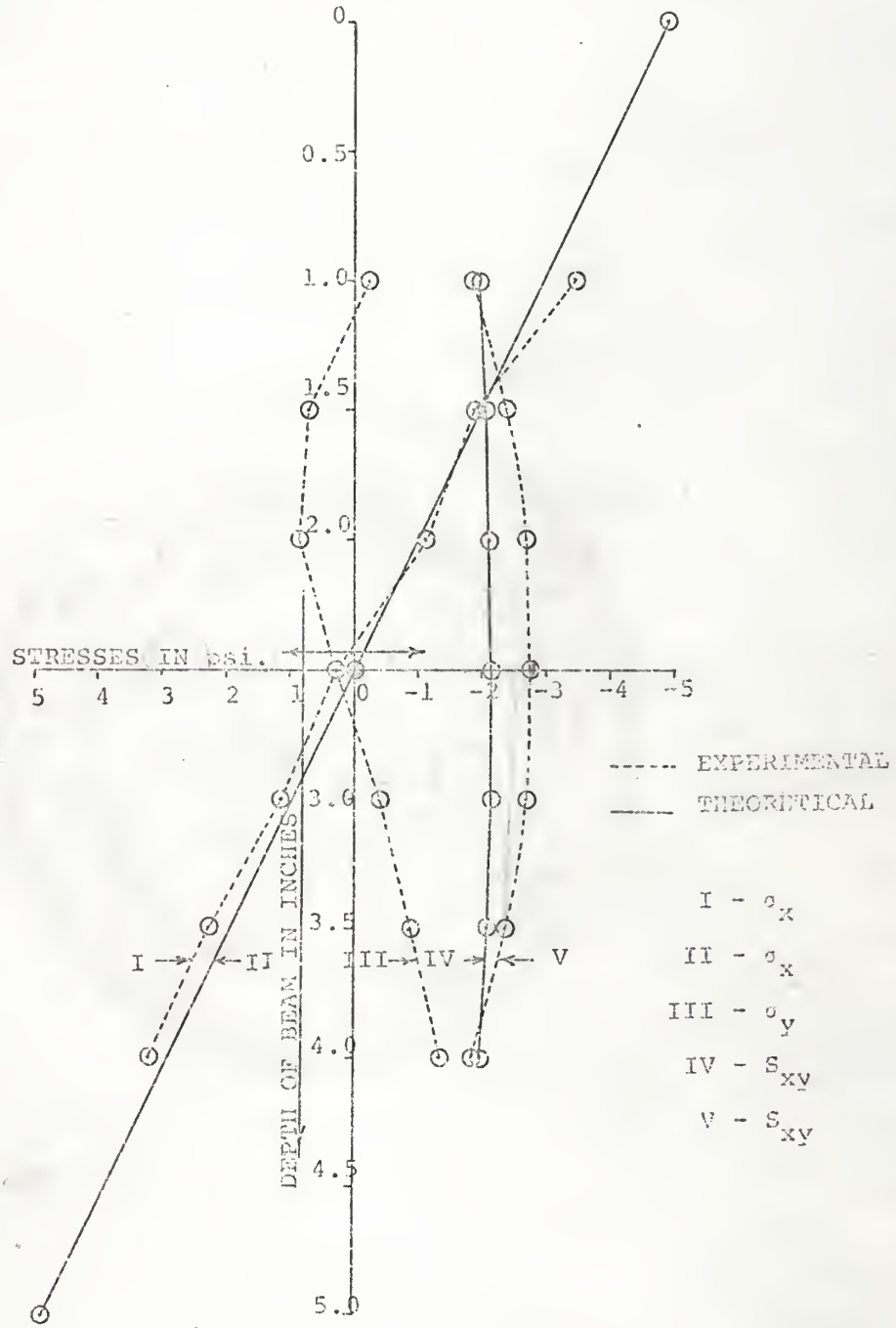

FIGURE 42. STRESS DISTRIBUTIONS FOR SECTION 5

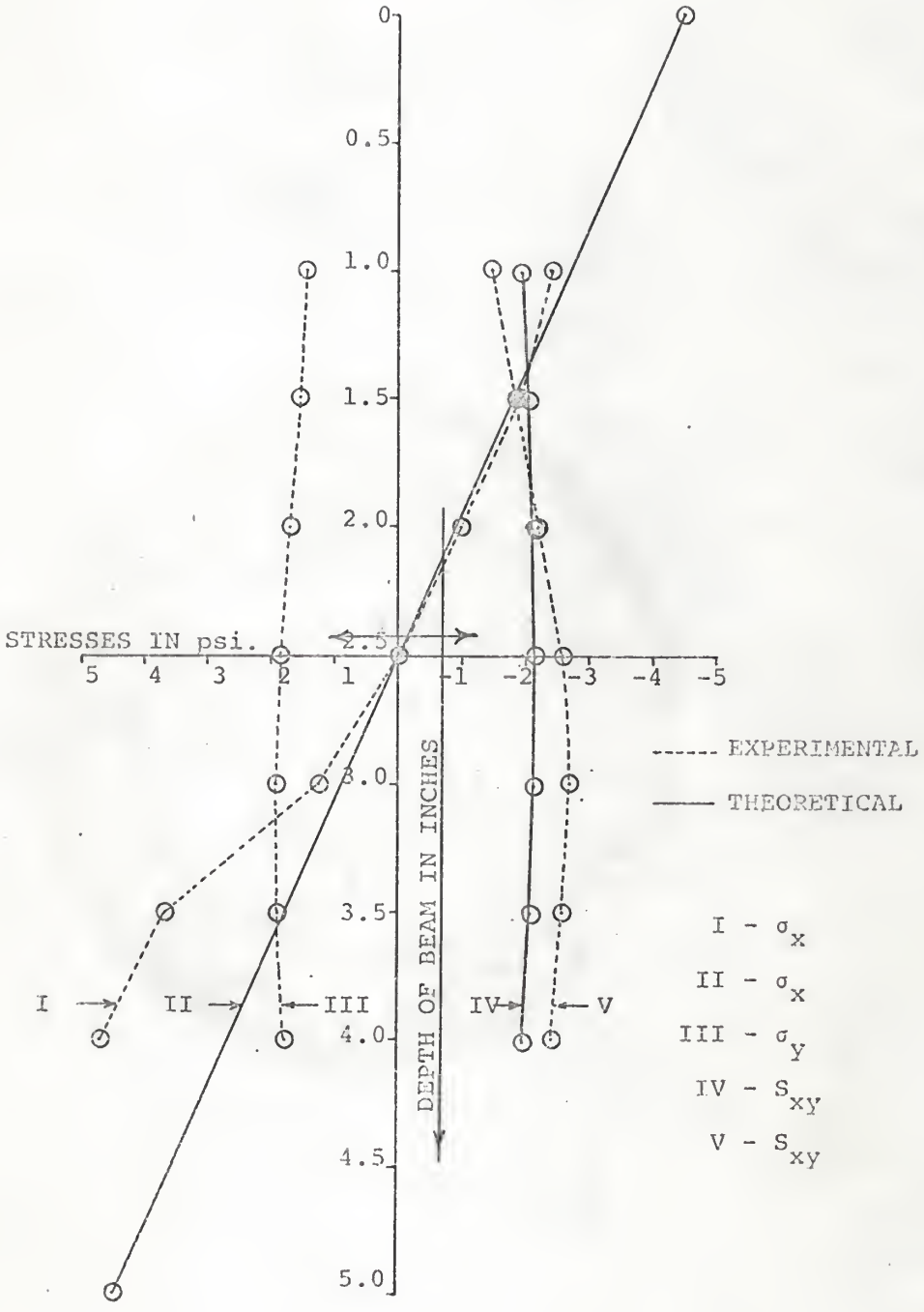

FIGURE 43. STRESS DISTRIBUTIONS FOR SECTION 6

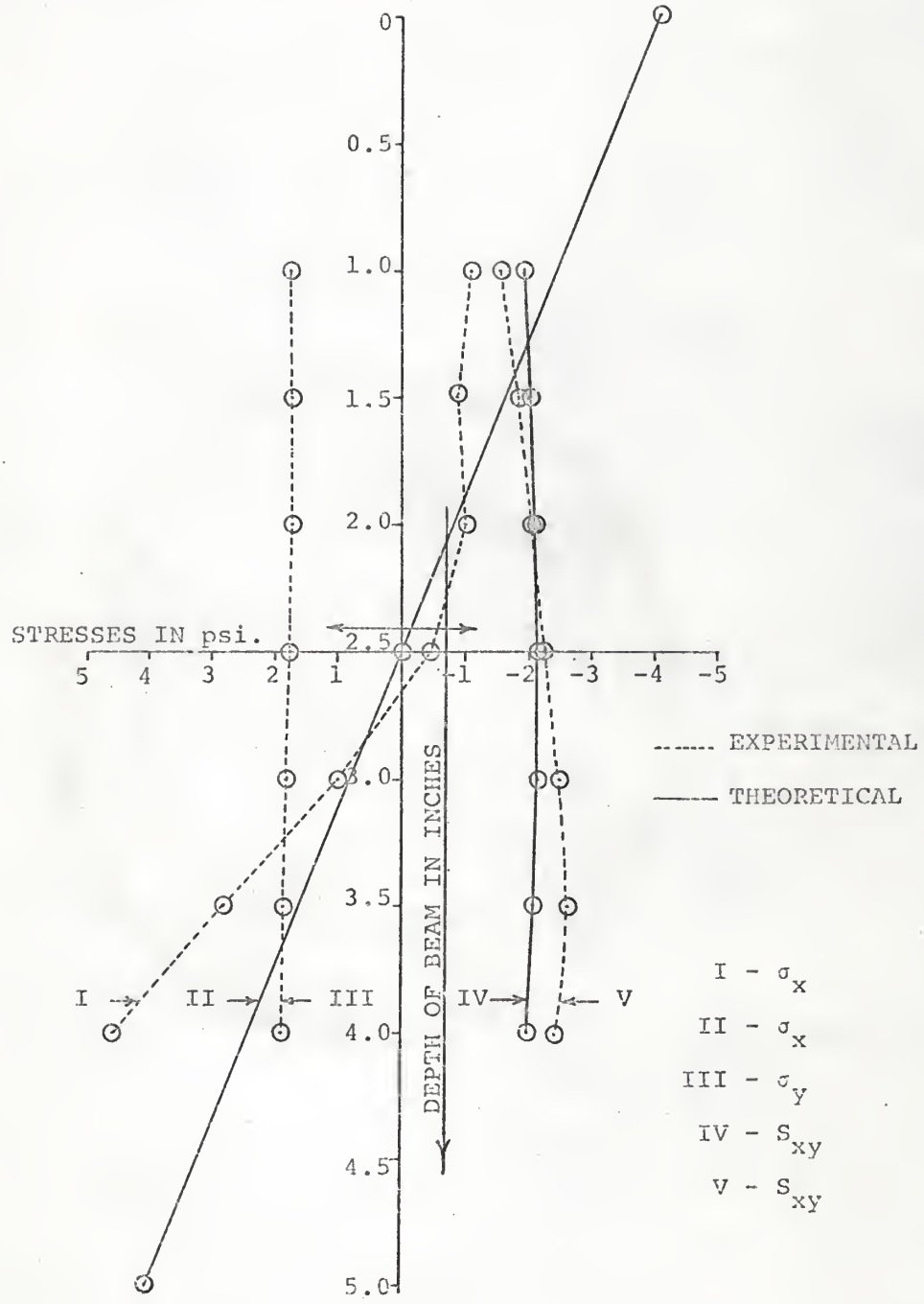

FIGURE 44. STRESS DISTRIBUTIONS FOR SECTION 7

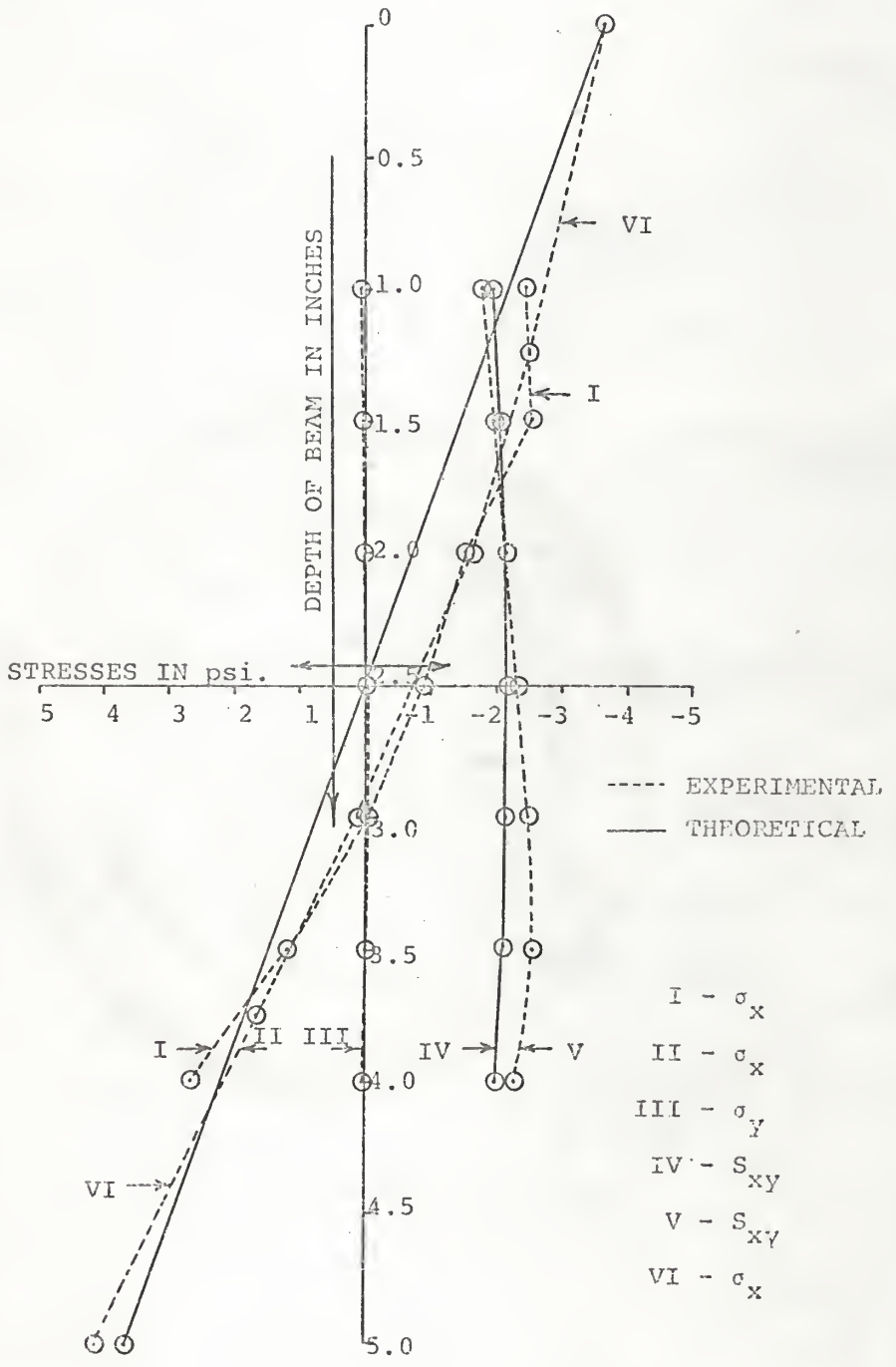

FIGURE 45. STRESS DISTRIBUTIONS FOR SECTION 8

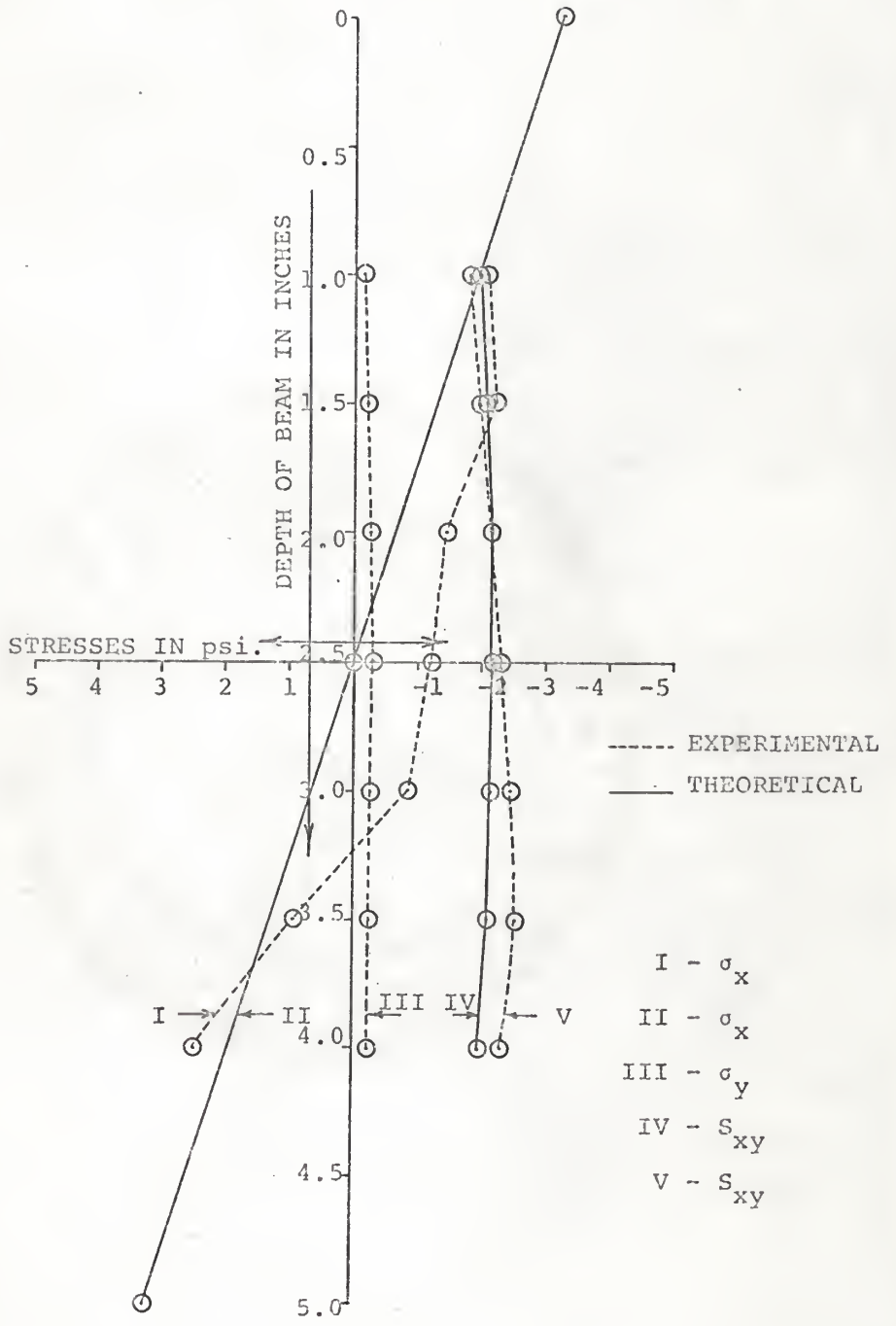

FIGURE 46. STRESS DISTRIBUTIONS FOR SECTION 9

DISCUSSION OF RESULTS

The photostress observations and the strain gage readings for the two positions of the beam were in good agreement. Therefore, the results obtained from the plastic on the left side of the beam would be duplicated if the calculations were carried on for the reversed position of the beam.

The calculations from the photostress data and strain gages at section 8 agreed quite well except for strain gage number 1' (Table 8). This gage showed a strain of +167 micro-inches whereas from photostress calculations it was found to be 191 micro-inches. This difference can be attributed to a number of sources of error, such as the mounting of the strain gage at that point, soldering of the terminals, birefringence reading, isoclinic angle reading etc., but in general the strain gage readings were in good agreement with the photostress calculations for section 8. Table 8 gives a comparison of the strain gage readings and the values obtained from the photostress readings for the vertical section 8.

The behavior of the beam can be visualized by examining the photostress observations and the isochromatic photographs (Fig. 11 through 13). The vertical sides of the hole were in compression, point (2,3), the upper corner of the hole, was also in compression and point (6,3), the lower corner of the hole, was in tension. It was further observed that an isotropic point existed between points (2,2) and (2,3) on the free boundary. This clearly indicated that the central portion of upper edge of the hole was in tension and behaved

TABLE 8. COMPARISON OF STRAIN GAGE AND PHOTOSTRESS RESULTS

STRAIN GAGE READINGS			PHOTO STRESS CALCULATIONS			
GAGE NO.	CO-ORDINATES IN INCHES	STRAIN ϵ_x IN MICRO-INCHES	LONGITUDINAL STRESS σ_x psi	TRANSVERSE STRESS σ_y psi	STRAIN $\epsilon_x = \frac{1}{E}(\sigma_x - \mu\sigma_y)$ IN MICRO-INCHES	STRAIN ϵ_x (NEGLECTING σ_y) IN MICRO-INCHES
8	(6, 1.25)	-248	-2480	+40	-249	-248
9	(6, 2)	-161	-1530	-10	-153	-153
0'	(6, 3)	+ 11	- 25	-25	- 1	- 1
1'	(6, 3.75)	+167	+1910	+32	+190	+191

independently as a T-beam under the action of the central load. (An exaggerated deflected shape of the hole is shown in Fig. 47.) Further, the upper corners of the hole showed a high concentration of stresses (Fig. 11). This stress concentration and the compression of the vertical sides of the hole put the web into transverse tension. At section 5, the transverse stress, σ_y, changed its sign. The upper portion of the web was in transverse tension and the lower portion was in transverse compression. The transverse stress along the vertical side of the hole varied from a maximum at the top to zero at the bottom corner. This put the upper portion of the web in transverse tension and the lower portion in transverse compression at section 5, the web at sections 6 and 7 was in transverse tension whereas section 9 indicated a small transverse compression. Section 8 showed almost zero transverse stress.

The neutral axis of the beam was above the centroidal axis at section 5 by 0.10 inch. At section 6, it almost coincided with the neutral axis while at section 7 it was below the neutral axis by 0.15 inch. The neutral axis at section 8 was below the centroidal axis by 0.5 inch and at section 9 it was below the centroidal axis by 0.725 inch. For a section at the vertical edge of the hole, the longitudinal stress was zero along the vertical edge of the hole. The vertical edges of the hole behaved as neutral surfaces for longitudinal stress, σ_x. Further, the strain gages on the flanges at section 8 showed that the compression flange was under less

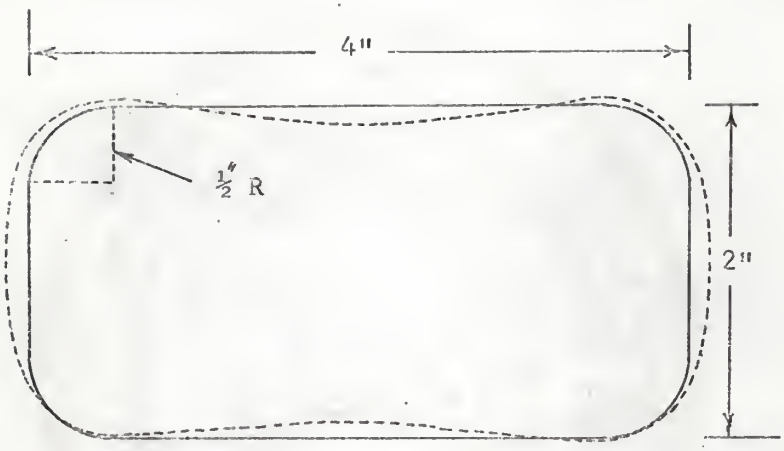

FIGURE 47. SKETCH SHOWING DEFLECTED SHAPE OF THE HOLE

longitudinal strain than the tension flange. This indicated that the neutral axis should shift downwards in order to maintain that section in equilibrium.

The behavior of the beam stated above appears to be peculiar due to the fact that some of the assumptions made in obtaining the usual stress distribution with the common flexure theory do not hold in the present situation. The first violation is that there was an abrupt change in the section of the beam, while it is assumed in the flexure theory that there are no abrupt changes in the section. In the present case there was a rectangular hole in the center of the beam and the edges of the hole had stress parallel to their surface only. Thus, the longitudinal stress at the vertical edges of the hole was zero. This behavior of the free surface disturbed the normal distribution of the stresses in the beam.

Another basic and important assumption, that plane sections remain plane after bending, is being violated in the present situation. Plane sections remain plane after bending in the case where shear forces at all the sections are zero; i.e., pure bending or where shear stress distribution remains the same at all the sections. In other words, it is assumed that the shears do not take any part in producing fiber strains. In the present case although the shear force was the same at all sections, the distribution of shear stresses at corresponding points for different sections was not the same. It varied from section to section as shown by the photostress calculations. This was explicitly due to the presence of the

hole. Since the shear stresses at the two faces of the elements were not equal, the shear stresses did take part in producing fiber strains.

Some of the other assumptions are not completely satisfied and these assumptions become more critical in the case of short beams (span to depth ratio being less than 10, Ref. 15). In the present case, the span to depth ratio was 6, therefore, the ratio of shear to moment was quite high. Thus, the present situation was that of a short beam. Hence the ordinary formulas, based on simple beam theory, for calculating the normal stresses are not truly applicable in the present case. In all such cases the analytical solutions become tedious and involved and experimental methods such as the photo-elastic method become very useful and suitable for stress analysis.

CONCLUSIONS

The presence of a rectangular hole in the web of an I-beam subjected to a central concentrated load leads to an interesting elastic stress distribution in the web. Due to the presence of the rectangular hole, the elastic stress distribution obtained from the experimental results did not agree with the stresses computed on the basis of simple beam theory. The neutral axis for the various sections of the beam did not coincide with the centroidal axis of the beam. At section 5 the neutral axis was above the centroidal axis and at section 6 it coincided with the centroidal axis of the beam. The neutral axis shifted below the centroidal axis of the beam at sections 7, 8 and 9 indicating that the fiber stresses below the neutral axis increased more rapidly as the distance from the neutral axis increased. The curves of shear stress distribution also indicated that the point of maximum shear stress was above the center of the beam at section 5, and at sections 6, 7, 8, 9 and 10 it was below the center of the beam.

From the comparison of strain gage calculations and the photostress calculations it may be concluded that the shear-difference method provides a very good tool for computing the stresses at the interior points of a structure. It is also concluded that the birefringent coating technique and photoelastic method of experimental stress analysis was found to be quite effective.

SUGGESTIONS FOR FURTHER RESEARCH

In the present study the elastic stress distribution from the edge of the opening to section 7" from the center of the beam has been obtained for a concentrated central load. This study can be extended to obtain elastic stress distribution for the full span of the beam. Moreover, the distribution of stresses for the beam can be obtained for different load positions to study the effect of a moving load. Various sizes of holes and different combinations of banding moment and shearing force can be investigated.

Another important topic of study would be to investigate the stress field in the immediate vicinity of the hole in the web. This investigation can lead to the study of various other shapes of holes. The various reinforcement requirements for the hole can be studied and the most effective and economical reinforcement can be obtained from it.

LIST OF SYMBOLS

C	- Birefringent reinforcing factor
E_s	- Modulus of Elasticity of the structure; i.e., aluminum alloy 6061-T6
I	- Moment of Inertia
K	- Strain Optical Sensitivity Constant of the Plastic
M	- Bending Moment
N_n	- Fringe Order in Normal Incedence
Q	- Static Moment of the remaining area about the neutral axis
S	- Section Modulus
S_{xy}	- Shear Stress in the X-Y plane
S_{max}	- Maximum Shear stress
V	- Shear Force
b	- Width of the section
c	- Velocity of light in vacuum
f	- Fringe Value
n	- Frequency
t_p	- Thickness of the Plastic
y	- Distance of the fiber from the Neutral Axis
λ	- Wave-length of light in inches
δ_n	- Relative Retardation in inches
ϵ_1	- Maximum Principal Strain
ϵ_2	- Minimum Principal Strain
σ_1	- Major Principal Stress
σ_2	- Minor Principal Stress

$(\varepsilon_1-\varepsilon_2)$ - Principal Strain Difference

$(\sigma_1-\sigma_2)$ - Principal Stress Difference

μ_s - Poisson's Ratio of the structure; i.e., aluminum alloy 6061-T6

σ_x - Normal Stress in the X-direction

σ_y - Normal Stress in the Y-direction

$(\sigma_x)_0$ - Normal Stress in the X-direction at a known point

$(\sigma_y)_0$ - Normal Stress in the Y-direction at a known point

Δx - Increment in the X-direction

Δy - Increment in the Y-direction

θ - Isoclinic Angle

ΔS_{xy} - Increment of shear stress

ACKNOWLEDGEMENT

I wish to express my sincere appreciation for the valuable guidance and encouragement given by Dr. Robert R. Snell, Associate Professor of Civil Engineering at Kansas State University. Without his efforts this research would not have been possible

I would like to extend my sincere thanks to Dr. Jack B. Blackburn, Head of the Civil Engineering Department at Kansas State University, for his valuable suggestions in the organization and review of this thesis.

REFERENCES

1. Morley, Will J., "Photo-elastic Analysis of I-beams with Elliptical Web Cut-outs." Experimental Mechanics, Vol. 1, No. 11, Nov. 1961.
2. Segner, E. P. Jr., "Reinforcement Requirements for Girder Web Openings." Jour. of Str. Div. ASCE, Vol. 90, No. ST 3, June 64, Part I.
3. Wahl, A. M.; Beenwkes, R., "Stress Concentration Produced by Holes and Notches." Trans. ASME, Vol. 56, 1934.
4. Frocht, M. M., "Photo-elasticity," Vol. I. John Wiley & Sons, Inc., March, 1941.
5. Hendry, A. W., "The Stress Distribution of a Simply Supported Beam of I-section Carrying a Central Load." Proc. Soc. for Exp. Stress Analysis, Vol. 7, No. 2, 1950.
6. Shawki; Hendry, A. W., "Stresses in a Deep Beam with Central Concentrated Load." Experimental Mechanics, Vol. I, June, 1961.
7. Duffy, J. "Effect of Thickness of Birefringent Coatings." Experimental Mechanics, Vol. 8, No. 1 , March 1961.
8. Post, D. and Zandman, F., "Accuracy of the Birefringent Coating Method for Coatings of Arbitrary Thickness," Experimental Mechanics, Vol. 18, No. 1, Jan. 1961.
9. Redner, S. S., Zandman, F. and Reigner, E. I., "Reinforcing Effect of Birefringent Coatings." Experimental Mechanics, Vol. 19, No. 1, Feb. 1962.

10. Shimada, S., "Photo-elastic Investigation of Stresses in Bars with Reinforced Semi-circular Notches in Bending." Experimental Mechanics, Vol. 2, No. 3, March, 1962.

11. Snell, R. R., "Reinforcement Requirements for Rectangular Openings in the Plates," Jour. of Str. Div. ASCE Vol. 91, No. ST4, Aug, 1965, Part I.

12. Vodivic, Fridric, "Contribution to the Analysis of Errors in Photo-elasticity." Experimental Mechanics, Vol. 5, Dec. 1965.

13. "Aluminum Construction Manual", Aug, 1959 by the Aluminum Association, New York.

14. "Budd Company, Instruments Division", Phoenixville, PA.
    (a) Instruction Manual for the Photostress Large Field Meter and its Accessories (Model LF/MU).
    (b) Instruction Manual for Digital Strain Indicator (Model A - 110).
    (c) Operating Manual for Strain Gage Switch and Balance Unit (Model C-10T and C-10LTC).
    (d) Instruction Manual for Printer Control (Model E-110).
    (e) Instruction Bulletin IB 8004.
    (f) Sales Bulletin BN 8002.
    (g) Technical Data Sheet D-02-30.

15. Withey and Maurer, "Strength of Materials," Second Edition, John Wiley & Sons, Inc. New York, 1935.

16. "Alcoa Aluminum Hand Book", by the Aluminum Company of America, Pittsburgh, PA.

17. Coker and Filon, "A Treatise on Photo-elasticity". Cambridge University Press, 1957.

18. Frocht, M. M., "The Shear-Difference Method," Proceedings 13th Eastern Photo-elasticity Conference, 1941.

19. Hetenyi, M., "Hand Book of Experimental Stress Analysis," John Wiley & Sons, Inc., 1950.

20. Heywood, R. B., "Designing by Photo-elasticity," Chapman & Hall, Ltd. London, 1952.

21. Jessop and Harris, "Photo-elasticity." Dover Publications, Inc., New York, 1949.

22. Swin, G. N., "Spannungerhohung Am Rande Von Lochern." Veb verlag Technik Berlin, 1956.

23. William T. Bean, "Strain Gage Accessories and Techniques."

EXPERIMENTAL STRESS ANALYSIS OF AN I-BEAM WITH A RECTANGULAR WEB CUT-OUT

by

JASBIR SINGH ARORA

B. Sc. in Engineering (Civil) Hons., Panjab University,
INDIA, 1964.

AN ABSTRACT

submitted in partial fulfillment of the

requirements for the degree

MASTER OF SCIENCE

Department of Civil Engineering

KANSAS STATE UNIVERSITY
Manhattan, Kansas

1967

In the present study, a photostress technique of stress analysis was used to investigate the elastic distribution of stresses in an aluminum alloy I-beam with a rectangular web opening at the center, when subjected to a central concentrated load. A Large Field Meter was used to take birefringence and isoclinic angle readings and the shear-difference method was used to obtain distribution of shear and normal stresses. The longitudinal stress distribution for one section was also obtained by the use of electric-resistance strain gages and was in good agreement with the one obtained from photostress observations.

The neutral axis for various sections of the beam did not coincide with the centroidal axis of the beam. At section 5 the neutral axis was above the centroidal axis and at section 6 it coincided with the centroidal axis of the beam. At sections 7, 8, and 9 the neutral axis was below the centroidal axis. The curves of shear stress distribution also indicated that the point of maximum shear stress was above the center of the beam at section 5, and at sections 6, 7, 8, 9 and 10 it was below the center line of the beam. This explicitly was due to the presence of a discontinuity in the web of the beam. By the comparison of the results obtained from photostress and strain gage readings, it was concluded that the shear-difference method and hence the photostress technique provide a very good tool for the analysis of stresses in such members.